*Clay Minerals*, (2017) **52**, 161–190

# A strontium isotope and trace element geochemical study of dolomite-bearing bentonite deposits in Bavaria (Germany)

MATHIAS H. KÖSTER[1,*], STEFAN HÖLZL[2] AND H. ALBERT GILG[1]

[1] *Lehrstuhl für Ingenieurgeologie, Technische Universität München, Arcisstr. 21, Munich 80333, Germany*
[2] *RiesKraterMuseum Nördlingen, Eugene-Shoemaker-Platz 1, Nördlingen 86720, Germany*

(*Received 16 September 2016; revised 30 December 2016; Editor: Helge Stanjek*)

ABSTRACT: The Landshut bentonites that formed from Ca- and Mg-poor rhyolitic tuffs in a fluviatile-lacustrine depositional environment of the Miocene Upper Freshwater Molasse, southern Germany, contain abundant palustrine, pedogenic and groundwater carbonates. Geochemical analyses of dolomites, calcites and smectites from bentonites of various environments by X-ray diffraction, thermal ionization mass spectrometry, inductively coupled plasma-mass spectrometry, and handheld X-ray fluorescence yield new insights into the compositions of fluids and sources of imported components involved in carbonate formation and bentonitization, as well as the timing of bentonite formation. Evaporated, Sr-rich brackish surface water with a molar Mg/Ca ratio of 2–5, derived mostly from the weathering of detrital carbonates, was involved in dolomite and bentonite formation in palustrine and some pedogenic environments. However, Sr-poor groundwater with a molar Mg/Ca ratio of ~ 1 and a stronger silicate weathering component caused bentonite and calcite formation in strictly pedogenic and groundwater settings. The $^{87}Sr/^{86}Sr$ and molar Mg/Ca in the smectite interlayers indicate later cation exchange with water having more radiogenic Sr sources and smaller molar Mg/Ca ratios. The Rb-Sr data indicate the common presence of detrital illitic phases in the <0.2 μm fractions of the bentonites. Cogenetic palustrine dolomite and a single smectite residue sample which lacks this detrital illitic phase provide an age constraint for bentonitization at 14.7 ± 4.1 Ma identical to primary ash deposition. Thus a rapid onset of bentonitization of accumulated ash and dolomite formation in evaporation-driven wetland environments is indicated for the genesis of the Landshut bentonites.

KEYWORDS: bentonite, dolomite, calcite, strontium geochemistry, Rb-Sr dating.

Dolomite and calcite are excellent palaeoenvironmental indicators used for reconstructing marine and terrestrial sedimentary environments (Banner, 1995). Dolomite and calcite are also common impurities in bentonite deposits but have rarely been studied in any detail (Knechtel & Patterson, 1956, 1962; Vogt, 1980; Delgado, 1993; Decher *et al*., 1996; Köster & Gilg, 2015). To date, only mineralogical and stable isotope studies of dolomites or calcites were presented from bentonite deposits in the vicinity of the Mediterranean Sea at Cabo de Gata, Spain (Delgado & Reyes, 1993; Delgado, 1993) and Milos, Greece (Decher *et al*., 1996). However, the stable isotope values of carbonates and smectites in these bentonites are often not consistent with precipitation from the same fluid (Delgado & Reyes, 1993; Decher *et al*., 1996), and together with sedimentological evidence for dolomite formation during later subaerial exposure and the involvement of seawater during bentonite formation (Delgado, 1993) suggest no systematic genetic link of carbonate and bentonite formation.

Recently, Köster & Gilg (2015) provided the first systematic study of carbonates in the terrestrial

*E-mail: mathias.koester@tum.de
https://doi.org/10.1180/claymin.2017.052.2.01

bentonite deposits in southern Germany. They showed that authigenic dolomite and calcite can be used to reconstruct the environments of ash alteration. The microfabrics, and $\delta^{13}C$ and $\delta^{18}O$ values of dolomite and calcite reveal that the carbonates formed in pedogenic, palustrine and groundwater settings shortly after ash deposition and possibly during the onset of bentonitization (Köster & Gilg, 2015). The chemical composition of fluids, *i.e.* salinity, redox conditions, and source(s) of Mg and Ca ions necessary for widespread dolomite and calcite precipitation, as well as bentonitization, of the Mg- and Ca-poor rhyolitic tuffs (Ulbig, 1999; Gilg, 2005; Abdul-Aziz *et al*., 2010) are not well constrained, however.

Tracing the source(s) of alkaline earth metal ions for bentonite formation is especially problematic because the smectite interlayer is susceptible to cation exchange reactions. Strontium isotope geochemistry has rarely been applied, therefore, in bentonite studies, the work of Chaudhuri & Brookins (1979) on the Clay Spur and Otay bentonites being a notable exception. Chaudhuri & Brookins (1979) demonstrated that Sr in smectites (Clay Spur: 52.4–248.3 ppm; Otay: 48.2–117.4 ppm) is mostly (but not exclusively) exchangeable and that Rb is more firmly bound in smectite residues (Clay Spur: 4.1–6.9 ppm; Otay: 2.9–4.2 ppm). The contrasting $^{87}Sr/^{86}Sr$ of the residues (Clay Spur: 0.710–0.712; Otay: 0.712) and leachates (Clay Spur: 0.707; Otay: 0.709) and the very low Rb/Sr values in the residues (<0.08) could be interpreted to suggest a later cation exchange with less radiogenic Sr. Chaudhuri & Brookins (1979), however, did not compare the Sr isotope ratios of smectites to diagenetic carbonates in the Clay Spur (Knechtel & Patterson, 1956, 1962) or in Otay (Cleveland, 1960) bentonites.

The intimate association of dolomites and calcites with bentonites in southern Germany (Köster & Gilg, 2015) is an excellent opportunity for further exploring dolomite and calcite formation in terrestrial bentonite deposits. We aim to ascertain the salinity and Mg/Ca of the fluids involved, the Sr (and by inference Ca and Mg) sources for carbonate and bentonite formation, and the timing of bentonite deposit formation using acid-leach techniques and the Rb/Sr method.

## BACKGROUND

### *Geological setting*

The Landshut bentonite deposits (Fig. 1) are located in a 40 km×10 km tectonic block in the North Alpine Foreland Basin bordered by NW–SE striking fault

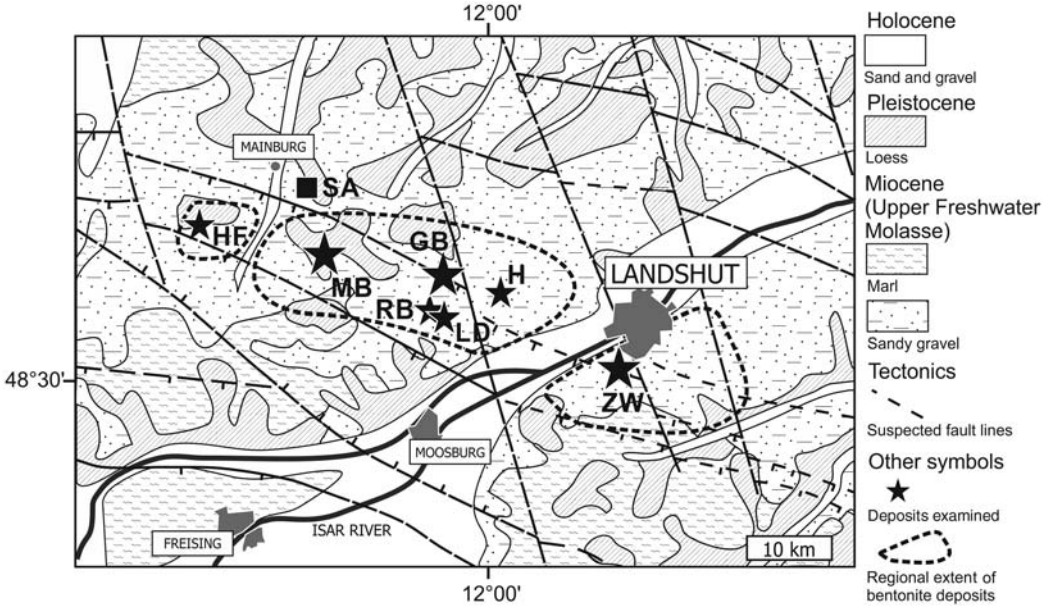


FIG. 1. Simplified geological map of the Landshut bentonite deposits (modified from Köster & Gilg, 2015; according to Freudenberger & Schwerd, 1996; Unger, 1999). Stars: Bentonite deposits. ZW – Zweikirchen, GB – Gabelsberg, MB – Mittersberg, LD – Landersdorf, H – Hader, RB – Rehbach, HF – Hofen. Square: Sandelzhausen (SA) fossil locality.

https://doi.org/10.1180/claymin.2017.052.2.01 Published online by Cambridge University Press

zones of a basement high (Unger, 1981, 1999; Abdul-Aziz *et al*., 2010). The deposits being mined at present are limited to the 14.7 ± 0.2 Ma main bentonite horizon (Abdul-Aziz *et al.*, 2010) in the upper part of the fluviatile Nördlicher Vollschotter (NV) sand and gravel unit and floodplain sediments of the Sand-Mergel-Decke (SMD) formed in an anastomosing to braided river system (Schmid, 2002; Maurer & Buchner, 2007) of the Upper Freshwater Molasse (UFM) (Vogt, 1980; Unger & Niemeyer, 1985; Unger *et al.*, 1990; Ulbig, 1999).

Ulbig (1999) invoked topographic "highs" and "lows" to explain sedimentological and depositional differences in the bentonites. Topographic "highs" are underlain by marl or clayey sand (SMD) and associated with abundant dolomite and calcite whereas topographic "lows" are characterized by sandy to gravely (NV) footwalls, higher detritus and lower carbonate content (Ulbig, 1999). All deposits are capped erosionally by younger sediments (Figs 2, 3) and the hiatus is indicated by pedogenic features in bentonites. Carbonates in bentonites of both settings formed in palustrine, pedogenic or groundwater environments (Köster & Gilg, 2015).

The presence of carbonates, partially altered tuffs, and sharp redox fronts evident in the distinct colour contacts (*e.g.* yellow *vs.* blue) of the bentonites are important characteristics for distinguishing the depositional and alteration settings of bentonites. Bluish-grey, green-grey, yellow, brown and mottled redox facies can be differentiated (Vogt & Köster, 1978; Unger, 1981; Unger & Niemeyer, 1985; Unger *et al*. 1990; Ulbig, 1999; Köster & Gilg, 2015).

The UFM in the eastern part of the North Alpine Foreland Basin is characterized by sand- and gravel-rich sediments with minor marls and received significant clastic input in the form of crystalline and sedimentary rocks from the Alps, the Bohemian Massif and the Swabian Alb (Lemcke, 1988; Unger, 1996; Frisch *et al*., 1998). The clasts in sands and gravels comprise quartz, granite, gneiss and Alpine Bunter sandstone, as well as Mesozoic marine lime- and dolostones among other lithotypes (*e.g*. Unger, 1991). Lime and dolostone clasts are derived from various Mesozoic marine carbonate sequences, mainly but not exclusively from the Mid-Triassic Hauptdolomit Formation of the Alps and Jurassic carbonates of the Swabian Alb (Unger, 1991; McArthur *et al*., 2001; Zorlu, 2007; Geske *et al*., 2012).

Groundwaters in the Upper Freshwater Molasse are characterized by high cation concentrations (Egger *et al*., 1983). The water chemistry is influenced by carbonate and silicate weathering, as well as cation-exchange reactions with clays that are the source of high $Ca^{2+}$, $Mg^{2+}$ and $HCO_3^-$ (and minor $Na^+$) concentrations in Molasse basin groundwater (Egger *et al*., 1983; Wagner *et al*., 2003). The groundwaters in the Cenozoic sediments are characterized by variable $^{87}Sr/^{86}Sr$ values compatible with both marine carbonate- and silicate-derived Sr sources (Voerkelius *et al*., 2010). The Ca-Mg-$HCO_3$ waters of the Western Molasse basin have low Sr isotope ratios (0.70835–0.70965) typical of the weathering of marine carbonates (Waber *et al*., 2014), whereas waters of the Eastern Molasse basin are characterized by more radiogenic $^{87}Sr/^{86}Sr$ ratios (>0.710) related to a combination of carbonate and silicate weathering and an increasing influence of the Variscan basement of the Bohemian Massif (Tütken & Vennemann, 2009).

## MATERIALS AND METHODS

### *Sample origin*

Dolomite and calcite, bentonite, weakly altered tuff and quartz-rich tuffitic sandstone originate from the Gabelsberg (GB), Mittersberg (MB) and Zweikirchen (ZW) deposits, southern Germany (Fig. 1). Additional carbonate samples are derived from the Hofen (HF), Rehbach (RB), Hader (H) and Landersdorf (LD) deposits (Fig. 1). With the exception of new samples from Hofen, dolomite and calcite samples were studied previously by Köster & Gilg (2015). The lithostratigraphic positions of the 67 bulk carbonate samples used for handheld X-ray fluorescence (XRF) analysis are documented in deposited Table A2, available from http://www.minersoc.org/pages/e_journals/dep_-mat_cm.html.

### *X-ray diffraction*

Carbonates were dry-ground in an agate mortar. Whole-rock bentonite and tuffitic samples were ground in isopropanol using a McCrone micronizing mill. As an internal standard, 10 wt.% of ZnO was added to estimate the amount of amorphous volcanic glass in tuffitic samples. The <0.2 µm fractions (*i.e*. almost 'pure' smectites) were separated from bulk aliquots of bentonite and tuff by centrifugation. Random powder mounts and air-dried and ethylene-glycolated (EG) oriented mounts of the <0.2 µm fractions were characterized by X-ray diffraction analysis from 2 to 70°2θ (Phillips PW 1800, Cu-*K*α radiation). The Ca and Mg contents, and cation ordering (*i.e.* the

https://doi.org/10.1180/claymin.2017.052.2.01 Published online by Cambridge University Press

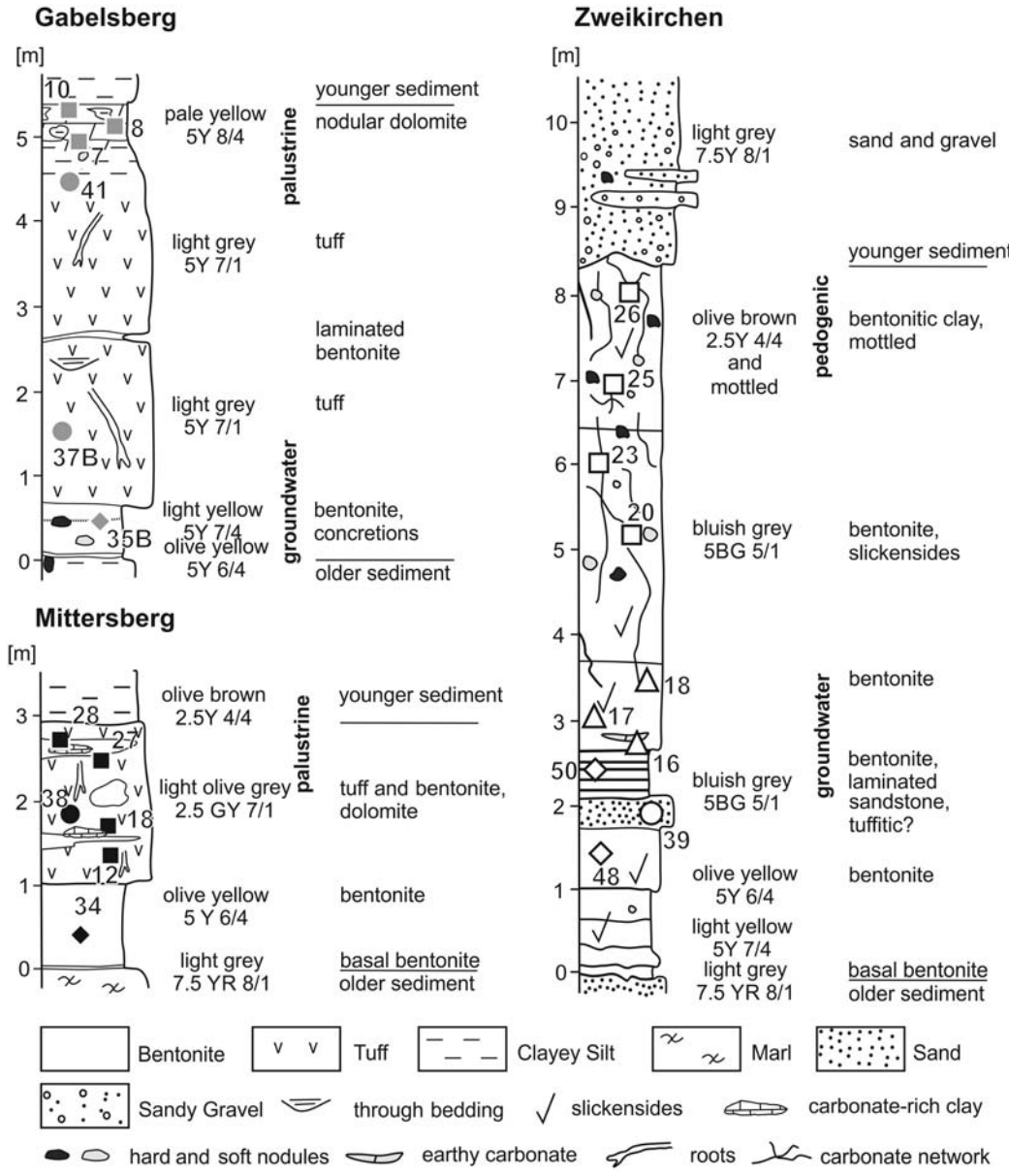


FIG. 2. Geological sections and sedimentary structures of the Gabelsberg (GB), Mittersberg (MB) and Zweikirchen (ZW) deposits. The samples used for ICP-MS and TIMS analysis are shown in the sections as squares (dolomite), triangles (calcite), diamonds (bentonite) or circles (partially altered tuff and a tuffitic sandstone [ZW39]) with sample numbers.

segregation of Ca and Mg into separate sheets) of dolomite were estimated using the $d_{104}$ reflection and the $d_{015}/d_{110}$ intensity ratio (Goldsmith & Graf, 1958; Lumsden & Chimahusky, 1980). Powder mounts were quantified by full-pattern Rietveld refinement using the *BGMNwin* 1.8.6. code with an estimated relative error of ~10 wt.%. Discrete illite was detected in the <0.2 μm fraction of three tuff samples and its content

https://doi.org/10.1180/claymin.2017.052.2.01 Published online by Cambridge University Press

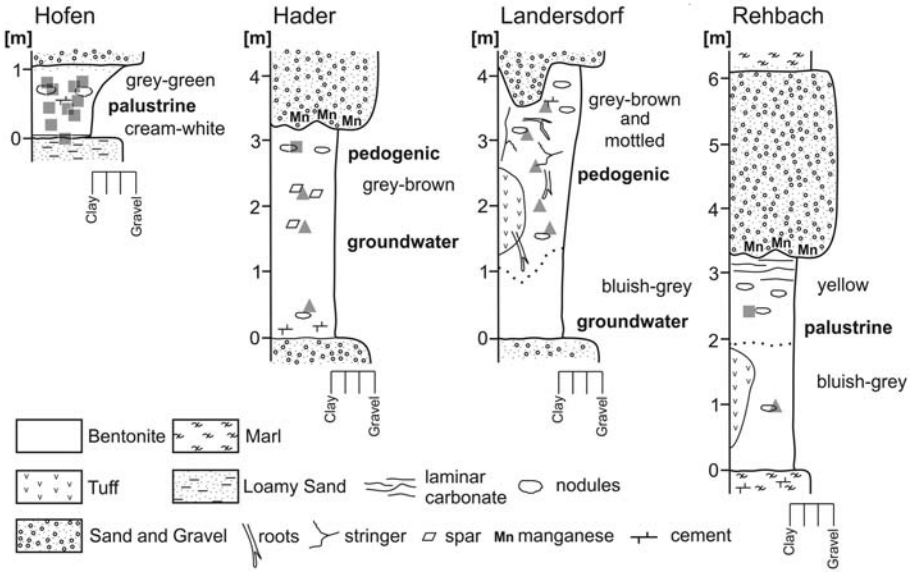


FIG. 3. Simplified geological sections with major sedimentary structures and carbonate accumulations in the Hofen (HF), Hader (H), Landersdorf (LD) and Rehbach (RB) deposits. Squares and triangles: p-XRF sample localities. Hofen base: ~1 cm cream-white basal bentonite layer ('Rahm').

was estimated using a reference intensity ratio (peak areas of $d_{001}$ reflections) of 4 for smectite and 1 for illite. The percentage of illite layers interstratified in smectite was determined according to Środoń (1980) using the peak migration method (26–28°2θ and 15–18°2θ). As discrete illite can interfere with the determination of the peak positions (Środoń, 1980), the percentage of illite layers interstratified in smectite was also estimated by the difference between the positions of 001/002 and 002/003 (Moore & Reynolds, 1997). Variable humidity, interlayer composition and layer charge can be problematic in determining the percentage of illite interstratified in smectite using these methods; a relative error of ~30% was estimated for the illite interstratified in smectite (Środoń, 1980).

### *Hydrochloric acid treatment and isotope geochemistry*

As previous mineralogical analyses showed (Table 1 present study, table 1 in Köster & Gilg, 2015) that the authigenic carbonates in bentonites contain variable amounts of silicates and oxides (*i.e.* clays, micas, feldspars, Fe- and Mn-minerals) carbonate samples with high carbonate contents and small amounts of all other minerals were selected and an acid-leach approach was applied. Prior to the hydrochloric acid treatment, both the carbonates and the <0.2 μm fractions of bentonites were dialysed with distilled water to remove soluble elements until the electrical conductivity remained at <0.9 μS/cm, and then were dried at 40°C, and split.

The carbonate samples were dissolved in 1 N HCl in teflon beakers after reaction at 20°C for 45 min. The solutions obtained from the dissolution of the carbonates were separated by centrifugation.

A simplified method was followed for the treatment of the <0.2 μm fractions (smectites) according to Chaudhuri & Brookins (1979), Clauer (1979) and Clauer *et al*. (1982) involving a two-step procedure. In the first step a weak hydrochloric acid treatment extracted the easily leachable, exchangeable and adsorbed elements. The second step involved a stronger acid attack to liberate more strongly bound elements, *e.g.* in illitic components and octahedral positions.

Smectites were first treated with triple distilled 1 N HCl for 15 to 20 min at 20°C and the solution was centrifuged and constituted the 'leachate'. The residual material (*i.e.* residue) was washed three times for 1 min each time with 1 N HCl with triple-distilled water to remove excess acid. The residue was then treated with 6 N HCl at 90°C for 12 h to extract the more strongly bound elements. The leachate and

https://doi.org/10.1180/claymin.2017.052.2.01 Published online by Cambridge University Press

TABLE 1. Mineral composition of carbonates, bentonite and tuff whole rocks (WR) and the <0.2 µm fractions used for Sr isotope analyses.

| Sample | Facies | Material | Type | Host lithology colour | Cal | Dol | Qz | Sme | Ilt/Ms | Kao/Chl | Fsp | Opal-CT | Amorph. |
|---|---|---|---|---|---|---|---|---|---|---|---|---|---|
| Zweikirchen | | | | | | | | | | | | | |
| ZW26 | ped | Dolomite | WR | mottled | T | 95 | 3 | 1 | 1 | 1 | | | |
| ZW25 | ped | Dolomite | WR | mottled | T | 99 | 1 | | | | | | |
| ZW23 | ped | Dolomite | WR | mottled | T | 77 | 11 | 8 | 3 | | | | |
| ZW20 | ped | Dolomite | WR | mottled | | 86 | 8 | 4 | 3 | | | | |
| ZW18 | gw | Calcite | WR | bluish-grey | 60 | 6 | 8 | 20 | 6 | | | | |
| ZW17 | gw | Calcite | WR | bluish-grey | 70 | | 5 | 19 | 6 | | T | | |
| ZW16 | gw | Calcite | WR | bluish-grey | 69 | T | 5 | 18 | 6 | 2 | | | |
| ZW50 | | Bentonite | WR | bluish-grey | | T | 6 | 76 | 8 | 3 | 6 | | |
| ZW50 | | Bentonite | <0.2 µm | bluish-grey | | | T | >99 | T | | | | |
| ZW39 | | Sandstone | WR | white-blue | | | 54 | 24 | 3 | 1 | 10 | 8 | |
| ZW39 | | Sandstone | <0.2 µm | white-blue | | | T | 84 | 16 | | T | | ? |
| ZW48 | | Bentonite | WR | yellowish | | T | 6 | 79 | 9 | 3 | 4 | | |
| ZW48 | | Bentonite | <0.2 µm | yellowish | | | T | >99 | T | | | | |
| Mittersberg | | | | | | | | | | | | | |
| MB28 | pal | Dolomite | WR | greenish-grey | | 74 | 1 | 13 | 4 | 1 | T | 8 | |
| MB27 | pal | Dolomite | WR | greenish-grey | | 75 | 1 | 13 | 3 | | | 8 | |
| MB18 | pal | Dolomite | WR | greenish-grey | | 66 | 3 | 21 | 6 | 1 | | 3 | |
| MB12 | pal | Dolomite | WR | greenish-grey | | 67 | 2 | 17 | 4 | 1 | | 9 | |

*(continued)*

TABLE 1. (*contd.*)

| Sample | Facies | Material | Type | Host lithology colour | Cal | Dol | Qz | Sme | Ilt/Ms | Kao/Chl | Fsp | Opal-CT | Amorph. |
|---|---|---|---|---|---|---|---|---|---|---|---|---|---|
| MB38 | | Tuff | WR | greenish-grey | | | 2 | 19 | 3 | 2 | 2 | | 73 |
| MB38 | | Tuff | <0.2 µm | greenish-grey | | | T | 90 | 10 | | | | ? |
| MB34 | | Bentonite | WR | greenish-grey | | | 3 | 83 | 4 | 6 | 4 | | |
| MB34 Gabelsberg | | Bentonite | <0.2 µm | greenish-grey | | | T | >99 | | | | | |
| GB10 | pal | Dolomite | WR | whitish-beige | 2 | 63 | 4 | 25 | 6 | | | | |
| GB08 | pal | Dolomite | WR | whitish-beige | 1 | 56 | 5 | 24 | 15 | | | | |
| GB07 | pal | Dolomite | WR | whitish-beige | 2 | 70 | 4 | 19 | 5 | | | | |
| GB41 | | altered Tuff | WR | greenish-grey | | T | 9 | 56 | 28 | | 2 | | 5 |
| GB41 | | altered Tuff | <0.2 µm | greenish-grey | | | T | >99 | T | | | | ? |
| GB37B | | Tuff | WR | beige | | | 6 | 25 | 4 | 2 | 4 | | 60 |
| GB37B | | Tuff | <0.2 µm | beige | | | T | XXX | X | | | | |
| GB35A | | Bentonite | WR | yellowish | | | T | 94 | 2 | | 4 | | |
| GB35a | | Bentonite | <0.2 µm | yellowish | | | T | >99 | | | | | |

ped = pedogenic, pal = palustrine, gw = groundwater. Cal = calcite, Dol = dolomite, Qz = quartz, Sme = smectite, Ilt/Ms = illite and/or muscovite, Kao/Chl = kaolinite or chlorite, Fsp = feldspar, Amorph. = X-ray amorphous (volcanic glass), XXX > 95%, X <5%, T = traces (<1%).

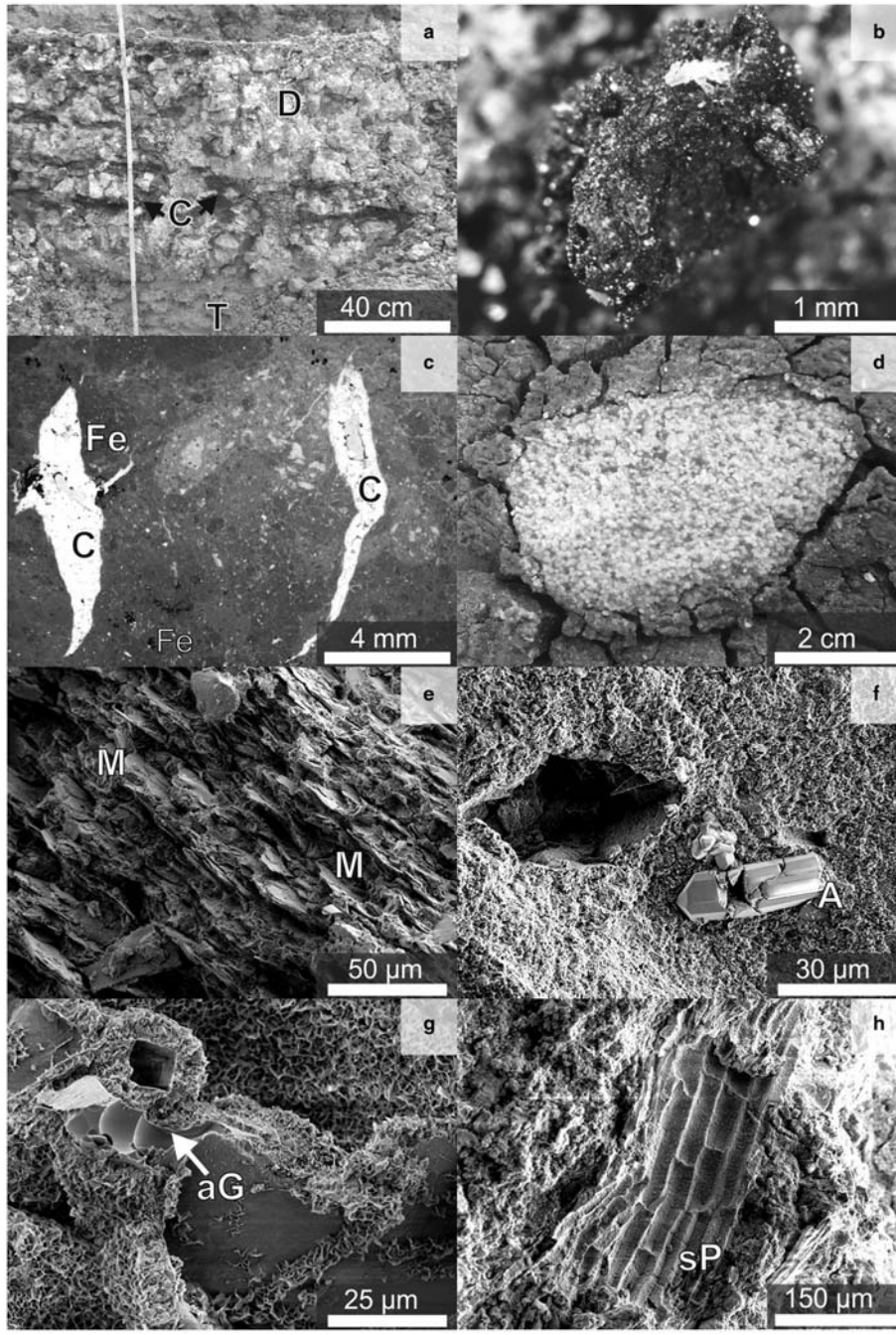


FIG. 4. Bentonite and carbonate fabrics. (a) Nodular palustrine dolomite (D) with clay patches (C) and partially altered tuff (T) in the Gabelsberg deposit (GB07, 08, 10). (b) Pyrite from bluish bentonite beds in the Rehbach deposit. (c) Calcite-spar (C) in shrinkage cracks with mottles of hematite and goethite (Fe) in the Landersdorf deposit. (d) Sugar-like groundwater calcite in the Hader deposit. (e) Bluish-grey (ZW50) bentonite with detrital mica (M). (f) Yellow bentonite (ZW48) with apatite crystal (A) both from Zweikirchen. (g) Almost completely altered volcanic glass (aG) with primary fabric preservation. (h) Silicified plant remains (sP) with preserved cell walls both from the Gabelsberg deposit (GB37B).

https://doi.org/10.1180/claymin.2017.052.2.01 Published online by Cambridge University Press

residue were analysed by inductively coupled plasma mass spectrometry (ICP-MS, Actlabs, Canada, UltraTrace 7; method A). As the Rb and Sr (and K) concentrations of method A were often below the detection limit but essential for the Sr isotope analysis, a second approach (method B) was used with a prolonged leaching time of 18 h and a Perkin Elmer DRC II ICP-MS at the Department of Geochemistry, University of Göttingen, Germany. The JA-2 standard (Japanese Andesite 2) was used in method B for external accuracy checking and showed an error of <10–30% relative to its average chemical composition (Imai *et al*., 1995). Results were corrected for drift caused by non-ionized material collected on the detector leading to erroneous counting of photons as ions, and for major oxygen interferences caused by argon from the plasma combining with oxygen interfering with the reliable detection of ions of a certain element. 100 mL of 2% $HNO_3$ with four internal standard elements (Be, Rh, In, Re) were added to 1 mL of the leachate and residue solutions obtained.

For Sr isotope analyses, the <0.2 μm fractions (of smectites) were leached according to method A and the carbonates were dissolved using 1 N HCl for 45 min at 20°C, as for the chemical analysis. The solutions were centrifuged using an Eppendorf MiniSpin S452 at 12,000×*g* to remove solids. An ion chromatographic column separation with Sr-specific crown-ether resin (Sr-Spec®, EIChroM Industries, USA) was used to extract Sr and to remove interfering elements such as Ca, Ba or Rb (Horwitz *et al*., 1992; Pin & Basin, 1992). Columns were pre-cleaned with 6.5 N $HNO_3$, 6 N HCl and triple-distilled $H_2O$, and flushed with 6.5 N $HNO_3$ after introduction of the sample solution. The Sr was finally eluted with 0.05 $HNO_3$.

The Sr isotope ratios of smectites and carbonates were determined using a thermal ionization mass spectrometer (MAT 261.5, Thermo Finnigan, Germany) in the ZERIN-lab at the Ries Crater Museum Nördlingen, Germany, using single tungsten filaments. Significant extant Rb (its evaporation and ionization temperature is lower than for Sr) was evaporated by controlled preheating before measurement, because traces of $^{87}Rb$ would interfere with the correct determination of the $^{87}Sr/^{86}Sr$ ratios. Isotope mass fractionation during analysis was corrected by referencing to an invariant $^{88}Sr/^{86}Sr$ value of 8.37521. To check for proper operation of the mass spectrometer, a certified reference material (SrCO3, NIST SRM 987) was measured and showed a mean $^{87}Sr/^{86}Sr$ of $0.710211 \pm 0.000023$ ($2\sigma$ of the mean; $n = 55$) during the time of analyses. The total analytical uncertainty (precision + accuracy) for $^{87}Sr/^{86}Sr$ in natural samples was estimated by replicate analyses of in-house standards (a red wine) at <50 ppm to verify the reproducibility of the complete sample-processing chain from digestion and extraction to measurement.

A split of a dolomite sample containing illite (MB28) was reacted for 24 h in 1 N HCl at 20°C to determine the influence of leaching time on isotope ratios. The Sr isotope ratio of MB28 increased only slightly from 0.710521 to 0.710541, indicating that leaching time has a negligible effect on the Sr isotope ratios of carbonates.

'Isochron' ages of smectite leachate and residue pairs (the <0.2 μm fractions) and carbonate-smectite residue pairs were calculated using *IsoPlot* 4.13 (Ludwig, 2008). The Rb/Sr ages were calculated using results from method A for leachates and results from method B for residues because the residue Sr

TABLE 2. Discrete illite and interstratified illite content of the <0.2 μm fractions.

| Sample | Host lithology | % discrete illite | °2θ smectite $d_{003}$ | °2θ smectite $d_{005}$ | % illite in smectite (Środoń, 1980) | $\Delta d2$ Smectite 001/003–002/003 | % illite in smectite (Moore & Reynolds, 1997) |
|---|---|---|---|---|---|---|---|
| ZW39 | Tuff | ~16 | 15.93 | 26.69 | 11 | 5.74 | 23 |
| ZW48 | Bentonite | | 15.62 | 26.25 | 1 | 5.40 | 4 |
| ZW50 | Bentonite | | 15.61 | 26.25 | 1 | 5.38 | 3 |
| MB34 | Bentonite | | 15.68 | 26.33 | 1 | 5.42 | 6 |
| MB38 | Tuff | ~10 | 15.87 | 26.63 | 12 | 5.48 | 9 |
| GB41 | Tuff | ~11 | 15.92 | 26.53 | 19 | 5.60 | 16 |
| GB35A | Bentonite | | 15.72 | 26.35 | 8 | 5.28 | 0 |

The error for the interstratified illite in smectite content is estimated at 10–30% (Środoń, 1980) and at 25% for discrete illite.

https://doi.org/10.1180/claymin.2017.052.2.01 Published online by Cambridge University Press

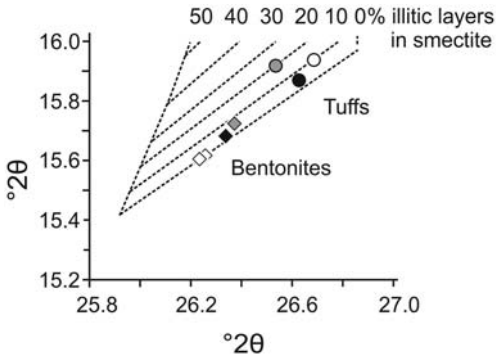


FIG. 5. Percentage of interstratified illite in smectite of the <0.2 μm fractions according to Środoń (1980). Diamonds: bentonite smectites; circles: tuff smectites. Mittersberg (black), Gabelsberg (grey) and Zweikirchen (white) deposits.

content was below the detection limit of method A. The decay constant used in the age calculations (Table 4) is $\lambda^{87}Rb = 1.42*10^{-11}$/y. The Sr and Rb concentrations were determined by ICP-MS as described above.

### *Portable X-ray fluorescence analysis*

A portable ED-XRF Bruker Tracer III-SD with a rhodium anode and a 10 $mm^2$ silicon drift detector, operating at 40 kV and 30 μA with the yellow filter (12 mil Al + 1 mil Ti), was used for chemical analysis of Ca, Sr and Mn on smoothed surfaces of carbonate samples. The spot size was ~3 mm× 4 mm. Measurements were conducted for 30 s. The spectra were fitted with the *ARTAX* software (Version 7.4.8.2) and calibrated using our ICP-MS results and the international standards BCS393, DWA-1, MAG-1 and NIM-S (Govindaraju, 1989). Average absolute errors (1 SD) are ±3.4 wt.% for CaO, ±45 μg/g for Sr and ±744 μg/g for Mn.

## RESULTS

### *Geological sections and sedimentary fabrics*

Bentonite deposits (Figs 2, 3) from pedogenic groundwater (ZW, LD, H) and palustrine (MB, GB, HF, RB) settings were distinguished based on the lithostratigraphic position of carbonates, carbonate mineralogy, microfabrics, stable isotope composition and colour (Köster & Gilg, 2015). The samples used for Sr isotope analysis are illustrated in Fig. 2.

Palustrine dolomites are characterized by nodular replacement beds (Fig. 4a), few but large nodules, dolomite-lined root moulds and soil churning (Köster & Gilg, 2015). Pedogenic dolomites and calcites are characterized by hard and soft nodules, earthy masses as well as stringer networks. Substantial calcite-spar is present in shrinkage cracks of pedogenic calcites (Fig. 4c). Groundwater carbonates form concentric or

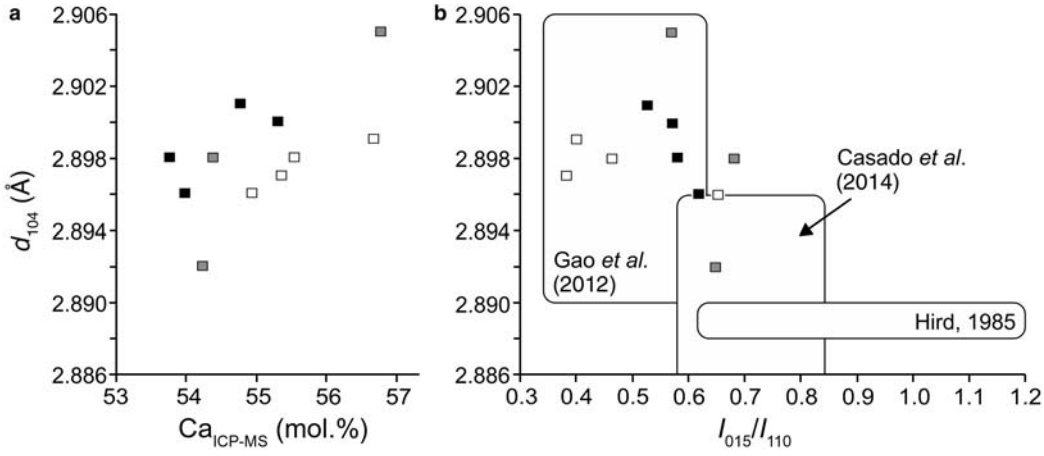


FIG. 6. Calcium content, $d_{104}$ positions and cation ordering of dolomites. (a) The $d_{104}$ reflection *vs.* calcium content. (b) Dolomite $d_{104}$ *vs.* the $I_{015}/I_{110}$ intensity ratios. Gao *et al.* (2012): Silurian, marine-overprinted lacustrine Ca-dolostones; Casado *et al.* (2014): Miocene lacustrine/palustrine Mg-dolomites; Carboniferous vein dolomites for comparison (Hird, 1985). Pedogenic: white (ZW); palustrine: black (MB) and grey (GB).

https://doi.org/10.1180/claymin.2017.052.2.01 Published online by Cambridge University Press

TABLE 3. Geochemical composition of carbonates, smectite leachates and residues according to method A.

| Sample No. | Facies | Material | MgO wt.% | CaO wt.% | $SiO_2$ wt.% | $TiO_2$ wt.% | $Al_2O_3$ wt.% | P wt.% | S wt.% | As µg/g | Ba µg/g | Co µg/g | Cs µg/g | Cu µg/g | Fe µg/g | Ga µg/g | K µg/g | Li µg/g | Mn µg/g | Na µg/g | Pb µg/g | Te µg/g | Th µg/g | U µg/g | V µg/g |
|---|---|---|---|---|---|---|---|---|---|---|---|---|---|---|---|---|---|---|---|---|---|---|---|---|---|
| Zweikirchen | | | | | | | | | | | | | | | | | | | | | | | | | |
| ZW26 | ped | Dolomite | 19.2 | 32.6 | 0.3 | <0.03 | 0.2 | <0.03 | 0.11 | <10 | 18 | 1.0 | 0.0 | <4.0 | <3.000 | 0.0 | n.d. | <6 | 373 | <500 | 3 | <10 | 0.4 | 3.0 | 10 |
| ZW25 | ped | Dolomite | 19.4 | 35.3 | 0.0 | <0.03 | 0.0 | <0.03 | 0.13 | <10 | 42 | 1.2 | 0.6 | <4.0 | <3.000 | 1.5 | n.d. | <6 | 357 | <500 | 4 | <10 | 0.5 | 4.6 | 30 |
| ZW23 | ped | Dolomite | 15.3 | 26.6 | 0.6 | <0.03 | 0.3 | <0.03 | 0.09 | <10 | 51 | 2.4 | 0.4 | <4.0 | <3.000 | 0.8 | n.d. | <6 | 1.210 | <500 | 19 | <10 | 1.5 | 4.1 | 20 |
| ZW20 | ped | Dolomite | 16.5 | 28.4 | 0.7 | <0.03 | 0.4 | 0.03 | 0.10 | <10 | 57 | 2.6 | 0.3 | 13 | 4.000 | 0.9 | n.d. | <6 | 1.700 | 900 | 20 | <10 | 0.8 | 4.1 | 10 |
| ZW18 | gw | Calcite | 1.9 | 38.8 | 0.7 | <0.03 | 0.3 | 0.08 | 0.14 | <10 | 56 | 1.6 | 0.6 | 9 | <3.000 | 1.0 | n.d. | <6 | 4.720 | 900 | 15 | <10 | 1.2 | 3.3 | 20 |
| ZW17 | gw | Calcite | 0.8 | 39.5 | 0.5 | <0.03 | 0.2 | 0.06 | 0.14 | <10 | 34 | 1.3 | 0.5 | <4.0 | <3.000 | 0.6 | n.d. | <6 | 3.550 | <500 | 10 | <10 | 1.2 | 1.1 | 10 |
| ZW16 | gw | Calcite | 1.2 | 43.2 | 0.4 | <0.03 | 0.2 | 0.03 | 0.16 | 10 | 65 | 2.2 | 0.5 | 6 | <3.000 | 0.7 | n.d. | <6 | 2.880 | <500 | 29 | <10 | 1.0 | 1.6 | 20 |
| ZW50 L | | Smectite | 0.5 | 0.7 | 0.2 | <0.03 | 0.1 | <0.03 | <0.05 | 10 | 12 | 1.8 | <0.02 | 13 | <3.000 | <0.4 | n.d. | <6 | <9 | <500 | 4 | <10 | 0.9 | <0.2 | 120 |
| ZW50 R | | Smectite | 1.5 | 0.1 | 0.1 | 0.03 | 5.5 | <0.03 | <0.05 | 50 | <6 | 6.1 | 1.1 | 16 | 19.590 | 6.8 | 605 | <6 | 40 | <500 | 15 | 250 | 7.1 | <0.2 | 500 |
| ZW39 L[a] | | Smectite | 0.4 | 0.5 | 0.1 | <0.03 | 0.1 | <0.03 | <0.05 | <10 | 32 | <0.04 | <0.02 | 12 | <3.000 | <0.4 | n.d. | <6 | <9 | <500 | 10 | <10 | 0.7 | 1.0 | 80 |
| ZW39 R[a] | | Smectite | 1.9 | 0.1 | 0.3 | <0.01 | 5.9 | <0.03 | <0.05 | 60 | 20 | 3.8 | 1.7 | 14 | 13.870 | 5.8 | 2.000 | <6 | 40 | <500 | 5 | 250 | 4.3 | 0.9 | 460 |
| ZW48 L | | Smectite | 0.4 | 0.4 | <0.1 | <0.03 | <0.09 | <0.03 | <0.05 | <10 | 62 | <0.04 | <0.02 | <4.0 | <3.000 | <0.4 | 368 | <6 | <9 | <500 | 6 | <10 | 0.5 | 0.5 | 110 |
| ZW48 R | | Smectite | 1.2 | 0.1 | 0.1 | 0.03 | 3.7 | <0.03 | <0.05 | 60 | 20 | 1.8 | 0.7 | 14 | 16.150 | 8.2 | 863 | <6 | 40 | <500 | 7 | 250 | 5.2 | <0.2 | 470 |
| Mittersberg | | | | | | | | | | | | | | | | | | | | | | | | | |
| MB28 | pal | Dolomite | 12.1 | 20.4 | 0.7 | <0.03 | 0.5 | 0.03 | 0.08 | 10 | 65 | 1.7 | 0.3 | 6 | <3.000 | 1.3 | n.d. | 13 | 305 | <500 | 8 | <10 | 2.3 | 5.8 | 30 |
| MB27 | pal | Dolomite | 15.0 | 25.7 | 1.1 | <0.03 | 0.7 | <0.03 | 0.09 | <10 | 74 | 2.3 | 0.4 | 8 | <3.000 | 1.2 | n.d. | 15 | 365 | <500 | 10 | <10 | 3.0 | 5.8 | 20 |
| MB18 | pal | Dolomite | 14.0 | 22.7 | 1.3 | <0.03 | 0.7 | <0.03 | 0.08 | <10 | 105 | 3.0 | 0.6 | 11 | <3.000 | 1.2 | n.d. | 14 | 386 | 500 | 18 | <10 | 3.8 | 2.3 | 20 |
| MB12 | pal | Dolomite | 14.2 | 23.1 | 1.2 | <0.03 | 0.7 | <0.03 | 0.08 | <10 | 88 | 2.2 | 0.4 | 8 | <3.000 | 1.2 | n.d. | 16 | 580 | 600 | 11 | <10 | 2.8 | 5.6 | 20 |

*(continued)*

TABLE 3. (*contd.*)

| Sample No. | Facies | Material | MgO wt.% | CaO wt.% | $SiO_2$ wt.% | $TiO_2$ wt.% | $Al_2O_3$ wt.% | P wt.% | S wt.% | As µg/g | Ba µg/g | Co µg/g | Cs µg/g | Cu µg/g | Fe µg/g | Ga µg/g | K µg/g | Li µg/g | Mn µg/g | Na µg/g | Pb µg/g | Te µg/g | Th µg/g | U µg/g | V µg/g |
|---|---|---|---|---|---|---|---|---|---|---|---|---|---|---|---|---|---|---|---|---|---|---|---|---|---|
| MB38 L[a] | | Smectite | 0.3 | 0.5 | 0.3 | <0.03 | 0.3 | <0.03 | <0.05 | 20 | 34 | <0.04 | <0.02 | 5 | <3.000 | <0.4 | n.d. | <6 | <9 | <500 | 5 | 50 | 0.6 | 0.0 | 190 |
| MB38 R[a] | | Smectite | 1.7 | 0.1 | 0.1 | 0.05 | 5.1 | <0.03 | <0.05 | 40 | 30 | 3.2 | 0.9 | 20 | 11.400 | 8.2 | 585 | 20 | 60 | <500 | 11 | 250 | 5.0 | <0.2 | 480 |
| MB34 L | | Smectite | 0.3 | 0.7 | <0.1 | <0.03 | <0.09 | <0.03 | <0.05 | 10 | 10 | <0.04 | <0.02 | <4.0 | <3.000 | <0.4 | n.d. | <6 | <9 | <500 | 2 | 50 | 0.6 | <0.2 | 190 |
| MB34 R | | Smectite | 1.9 | 0.1 | 0.2 | 0.05 | 5.8 | <0.03 | <0.05 | 60 | 0 | 6.3 | 0.4 | 12 | 19.700 | 9.2 | 836 | 20 | 60 | <500 | 10 | 250 | 8.2 | <0.2 | 480 |
| Gabelsberg | | | | | | | | | | | | | | | | | | | | | | | | | |
| GB10 | pal | Dolomite | 14.3 | 26.0 | 0.7 | <0.03 | 0.3 | 0.11 | 0.09 | <10 | 63 | 1.4 | 0.4 | 9 | <3.000 | 1.1 | n.d. | 15 | 437 | <500 | 3 | <10 | 2.1 | 7.1 | 20 |
| GB08 | pal | Dolomite | 17.2 | 28.4 | 1.3 | <0.03 | 0.9 | 0.06 | 0.10 | <10 | 84 | 5.5 | 0.5 | 8 | <4.000 | 1.2 | n.d. | 20 | 451 | 800 | 10 | <10 | 2.7 | 13.6 | 20 |
| GB07 | pal | Dolomite | 15.4 | 25.5 | 1.3 | <0.03 | 1.2 | 0.04 | 0.09 | <10 | 110 | 7.4 | 0.4 | 7 | <4.000 | 2.3 | n.d. | 19 | 372 | 800 | 8 | <10 | 1.6 | 10.2 | 10 |
| GB41 L | | Smectite | 0.3 | 0.9 | 0.1 | <0.03 | 0.3 | <0.03 | <0.05 | 20 | 8 | <0.04 | <0.02 | 5 | <3.000 | <0.4 | n.d. | <6 | <9 | <500 | 2 | 50 | 0.6 | 0.8 | 130 |
| GB 41 R | | Smectite | n.d. | n.d. | n.d. | n.d. | n.d. | n.d. | n.d. | n.d. | n.d. | n.d. | n.d. | n.d. | n.d. | n.d. | 2.118 | n.d. | n.d. | n.d. | n.d. | n.d. | n.d. | n.d. | n.d. |
| GB37B L[a] | | Smectite | 0.2 | 0.9 | 0.1 | <0.03 | <0.09 | <0.03 | <0.05 | <10 | 29 | 0.7 | <0.02 | 8 | <3.000 | 0.5 | n.d. | <6 | <9 | <500 | 3 | <10 | 0.7 | 0.4 | 130 |
| GB37B R[a] | | Smectite | 1.8 | 0.1 | 0.1 | 0.07 | 4.6 | <0.03 | <0.05 | 50 | 40 | 4.4 | 1.8 | 27 | 16.100 | 7.6 | 1.013 | 20 | 100 | <500 | 5 | 240 | 5.1 | 0.4 | 490 |
| GB35A L | | Smectite | 0.3 | 0.7 | <0.1 | <0.03 | <0.09 | <0.03 | <0.05 | <10 | 6 | <0.04 | <0.02 | <4.0 | <3.000 | <0.4 | 61 | <6 | <9 | <500 | <0.2 | <10 | 0.2 | <0.2 | 100 |
| GB35A R | | Smectite | n.d. | n.d. | n.d. | n.d. | n.d. | n.d. | n.d. | n.d. | n.d. | n.d. | n.d. | n.d. | n.d. | n.d. | 35 | n.d. | n.d. | n.d. | n.d. | n.d. | n.d. | n.d. | n.d. |

The detection limit of K, according to method A, was 5000 µg/g. The K content of the smectites was determined using method B. L = leachate, R = residue, n.d. = not determined, ped = pedogenic, pal = palustrine, gw = groundwater.
[a]Discrete illite in sample.

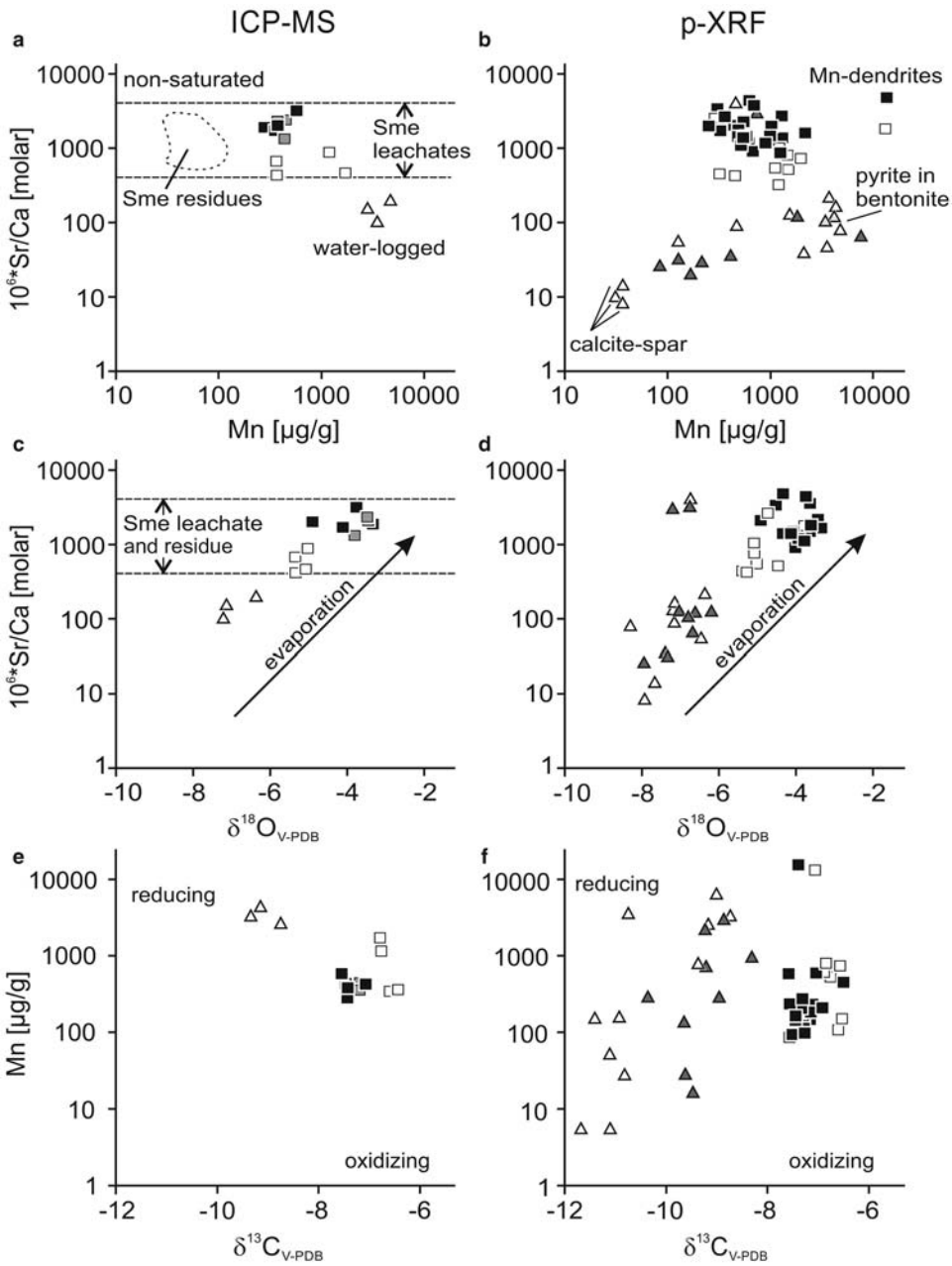


FIG. 7. Geochemical data of carbonates used for Sr isotope analysis using an HCl-leach method (left) and of bulk samples using portable XRF (side). (a, b) Sr/Ca *vs.* Mn content. (c, d) Sr/Ca *vs.* $\delta^{18}O$ values (Köster & Gilg, 2015). (e, f) Mn content *vs.* $\delta^{13}C$ values (Köster & Gilg, 2015). Squares: palustrine (black and grey) and pedogenic (white) dolomite. Triangles: groundwater (white) calcite. Note: not all samples measured by p-XRF were analysed for stable isotopes.

nodular masses of clotted micrite and limpid calcite-spar (Fig. 4d). Based on colour, three redox facies are distinguished: reduced blue bentonite, intermediate green, and oxidized yellow bentonite. Blue bentonites commonly contain pyrite (Fig. 4b) and appear either homogeneous or laminated because of detrital mica

https://doi.org/10.1180/claymin.2017.052.2.01 Published online by Cambridge University Press

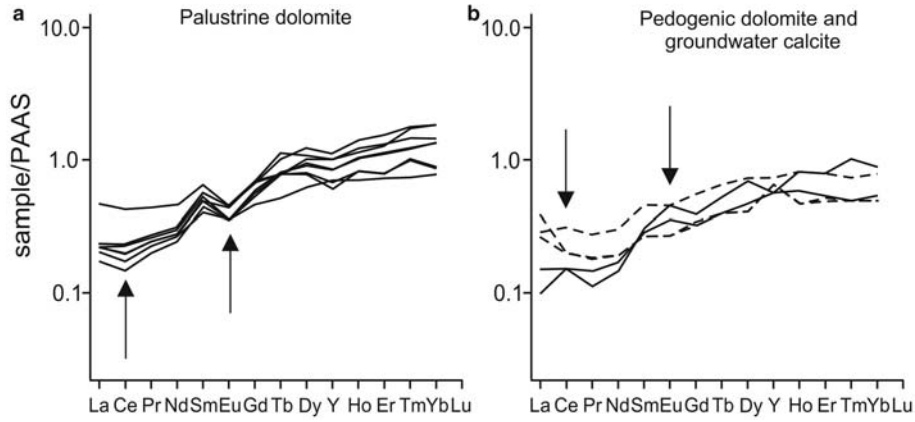


FIG. 8. *REE* + Y patterns of *HREE*-enriched dolomites and calcites. (a) Negative Ce and Eu anomalies (arrows) in palustrine dolomite. (b) Pedogenic (solid line) and groundwater calcite (dashed line) with variable Ce and Eu anomalies (arrows).

(Fig. 4e). Green and yellow bentonites were encountered solely as homogenous clay (Fig. 4f). Root traces and sedimentary fabrics are seldom preserved in bentonites. Partially altered tuff, however, shows excellent fabric preservation of deep-reaching roots (Köster & Gilg, 2015), altered volcanic glass shards (Fig. 4g) and silicified plant remains (Fig. 4h).

### *Mineralogical composition*

The mineralogical compositions of carbonates and the <0.2 μm fractions of bentonites and tuffs are shown in Tables 1 and 2. Well defined peaks at 2.892–2.905 Å and at 3.022–3.029 Å are characteristic for Ca-rich dolomite and Mg-enriched calcite, respectively. The $d_{015}$ and $d_{110}$ cation ordering reflections confirm the actual dolomite character and reveal a moderate degree of order (Fig. 6; $I_{015}/I_{110}$: 0.38–0.68). The Ca-rich composition and moderate cation ordering suggest a primary origin for the dolomite (Last, 1990).

Dioctahedral smectite ($d_{060}$; 1.50–1.49 Å) is the main constituent of bentonite and tuff, with variable amounts of mica/illite, kaolinite, chlorite, quartz, feldspar, volcanic glass, pyrite, goethite and hematite. Oriented, air-dried and ethylene-glycol solvated <0.2 μm fractions expand upon EG-treatment from 14.7 to 17.3 Å. Some of the <0.2 μm fractions (Table 2) contain traces of discrete illite/mica, visible as a small, low-angle reflection (001; ~10 Å). The <0.2 μm fraction of strongly altered tuff (GB41) is composed of R0 mixed-layer illite-smectite (I-S) with 20% illite layers. The tuffitic whole-rock samples (GB37B) and <0.2 μm fractions of tuff (GB41, MB38) and tuffitic sandstone (ZW39) contain larger amounts of discrete illite-mica, quartz, or opal-CT than bentonite. The percentage of interstratified illite in the I-S of the <0.2 μm fractions is illustrated in Fig. 5.

### *Chemical composition of dolomite and calcite*

The ICP-MS analyses of carbonates (Table 3) confirm the XRD results and reveal dolomites with Mg/(Mg + Ca) molar ratios of 0.45 ± 0.01 ($n$ = 11) and calcites with Mg/(Mg + Ca) molar ratios of 0.04 ± 0.02 ($n$ = 3).

The trace-element compositions of carbonates from the various environments show significant differences. Strontium concentrations in dolomites exceed those of most island dolomites (Budd, 1997) and are highest in the palustrine dolomites (536–1,120 μg/g) that have Rb concentrations (4.8–9.5 μg/g) similar to the pedogenic dolomites (Table 4). Palustrine dolomites have low Mn contents (305–580 μg/g) but elevated concentrations of Th and U. The palustrine dolomites also have elevated Li (13–20 μg/g) and Ba (63–110 μg/g) concentrations (Table 3). The pedogenic dolomites have intermediate Sr (208–368 μg/g) and Rb (1.4–8.5 μg/g) contents and Mn content (357–1700 μg/g; Tables 3 and 4). Calcites display much lower Sr (66–126 μg/g) but higher Rb (10.6–13.3 μg/g) and very high Mn (2880–4729 μg/g) concentrations (Tables 3 and 4).

The Ca, Sr and Mn concentrations determined by portable XRF (deposited Table A2, available from http://www.minersoc.org/pages/e_journals/dep_mat_cm.html) are dominated by carbonates, but are in part

https://doi.org/10.1180/claymin.2017.052.2.01 Published online by Cambridge University Press

TABLE 4. Rb and Sr content of carbonates (method A) and smectites (methods A and B), as well as Sr isotope ratios (method A) and leachate-residue model ages, including discrete (Ilt) and interstratified illite (Ilt/Sme) content according to Środoń (1980) and in brackets according to Moore & Reynolds (1997).

| Sample No. | Material | Rb µg/g | Sr µg/g | Rb/Sr | $^{87}Rb/^{86}Sr$ | 1 SD | $^{87}Sr/^{86}Sr$ measured | 2sigma_mean | $^{87}Sr/^{86}Sr_{initial}$ at 14.7 Ma | L (A) + R (B) model Age [Ma] | Ilt $^{87}Sr/^{86}Sr_{initial}$ | Ilt/Sme % | % |
|---|---|---|---|---|---|---|---|---|---|---|---|---|---|
| Zweikirchen | | | | | | | | | | | | | |
| ZW26 | Dolomite | 1.4 | 216 | 0.006 | 0.019 | 0.001 | 0.71108 | 0.000012 | | | | | |
| ZW25 | Dolomite | 8.5 | 368 | 0.023 | 0.067 | 0.004 | 0.71107 | 0.000024 | | | | | |
| ZW23 | Dolomite | 8.3 | 368 | 0.023 | 0.065 | 0.004 | 0.71105 | 0.000157 | | | | | |
| ZW20 | Dolomite | 7.7 | 208 | 0.037 | 0.107 | 0.007 | 0.71135 | 0.000023 | | | | | |
| ZW18 | Calcite | 13.3 | 126 | 0.106 | 0.306 | 0.020 | 0.71148 | 0.000020 | | | | | |
| ZW17 | Calcite | 11.7 | 66 | 0.177 | 0.513 | 0.033 | 0.71154 | 0.000018 | | | | | |
| ZW16 | Calcite | 10.6 | 109 | 0.097 | 0.282 | 0.018 | 0.71138 | 0.000013 | | | | | |
| ZW50 L, A | Sme/Bentonite | 1.4 | 23.0 | 0.061 | 0.176 | 0.011 | 0.71268 | 0.000019 | | | | | |
| ZW50 R, A | Sme/Bentonite | 7.0 | <10 | | | | 0.71522 | 0.000017 | | | | | |
| ZW50 R, B | Sme/Bentonite | 7.8 | 3.7 | 2.108 | 6.106 | 0.397 | 0.71522 | 0.000017 | 0.71395 | 30.2 ± 4.6 | 0.71261 ± 14 | | 1 (3) |
| ZW39 L, A[a] | Sme/Tuff | 4.1 | 30.0 | 0.137 | 0.396 | 0.026 | 0.71285 | 0.000013 | | | | | |
| ZW39 R, A[a] | Sme/Tuff | 23 | <10 | | | | 0.72286 | 0.000015 | | | | | |
| ZW39 R, B[a] | Sme/Tuff | 14.0 | 1.0 | 14.000 | 40.581 | 2.638 | 0.72286 | 0.000015 | 0.71440 | 17.6 ± 2.3 | 0.71275 ± 10 | 16 | 11 (23) |
| ZW48 L, A | Sme/Bentonite | 1.3 | 24.0 | 0.054 | 0.157 | 0.010 | 0.71231 | 0.000041 | | | | | |
| ZW48 R, A | Sme/Bentonite | 8.0 | <10 | | | | 0.71537 | 0.000009 | | | | | |
| ZW48 L, B | Sme/Bentonite | 3.1 | 90.1 | 0.034 | 0.100 | 0.006 | 0.71231 | 0.000041 | | | | | |
| ZW48 R, B | Sme/Bentonite | 14.0 | 3.3 | 4.242 | 12.288 | 0.799 | 0.71537 | 0.000009 | 0.71281 | 17.7 ± 2.9 | 0.71229 ± 30 | | 1 (4) |

*(continued)*

TABLE 4. (*contd.*)

| Sample No. | Material | Rb µg/g | Sr µg/g | Rb/Sr | $^{87}Rb/^{86}Sr$ | 1 SD | $^{87}Sr/^{86}Sr$ measured | 2sigma_mean | $^{87}Sr/^{86}Sr_{initial}$ at 14.7 Ma | L (A) + R (B) model Age [Ma] | Ilt $^{87}Sr/^{86}Sr_{initial}$ | % | Ilt/Sme % |
|---|---|---|---|---|---|---|---|---|---|---|---|---|---|
| Mittersberg | | | | | | | | | | | | | |
| MB28 | Dolomite | 5.3 | 606 | 0.009 | 0.025 | 0.002 | 0.71059 | 0.000021 | | | | | |
| MB27 | Dolomite | 7.8 | 686 | 0.011 | 0.033 | 0.002 | 0.71079 | 0.000020 | | | | | |
| MB18 | Dolomite | 9.5 | 714 | 0.013 | 0.039 | 0.003 | 0.71090 | 0.000014 | | | | | |
| MB12 | Dolomite | 6.9 | 1.120 | 0.006 | 0.018 | 0.001 | 0.71052 | 0.000010 | | | | | |
| MB12–24h | Dolomite | | | | | | 0.71054 | 0.000014 | | | | | |
| MB38 L, A[a] | Sme/Tuff | 3.1 | 12.0 | 0.258 | 0.748 | 0.049 | 0.71151 | 0.000025 | | | | | |
| MB38 R, A[a] | Sme/Tuff | 11.0 | <10 | | | | 0.71708 | 0.000014 | | | | | |
| MB38 R, B[a] | Sme/Tuff | 12.6 | 2.4 | 5.250 | 15.209 | 0.989 | 0.71708 | 0.000014 | 0.71391 | 27.1 ± 3.8 | 0.71123 ± 19 | 10 | 12 (9) |
| MB34 L, A | Sme/Bentonite | 0.9 | 11.0 | 0.082 | 0.237 | 0.015 | 0.71139 | 0.000017 | | | | | |
| MB34 R, A | Sme/Bentonite | 4.0 | <10 | | | | 0.71401 | 0.000010 | | | | | |
| MB34 R, B | Sme/Bentonite | 11.0 | 2.0 | 5.500 | 15.929 | 1.035 | 0.71401 | 0.000010 | 0.71069 | 11.8 ± 1.8 | 0.71135 ± 18 | | 1 (6) |
| Gabelsberg | | | | | | | | | | | | | |
| GB10 | Dolomite | 5.5 | 536 | 0.010 | 0.030 | 0.002 | 0.71061 | 0.000024 | | | | | |
| GB08 | Dolomite | 6.5 | 1.050 | 0.006 | 0.018 | 0.001 | 0.71113 | 0.001170 | | | | | |
| GB07 | Dolomite | 4.8 | 874 | 0.005 | 0.016 | 0.001 | 0.71042 | 0.000024 | | | | | |
| GB41 L, A[a] | Sme/altered Tuff | 1.5 | 8.0 | 0.188 | 0.543 | 0.035 | 0.71167 | 0.000027 | | | | | |

*(continued)*

TABLE 4. (*contd.*)

| Sample No. | Material | Rb µg/g | Sr µg/g | Rb/Sr | $^{87}Rb/^{86}Sr$ | 1 SD | $^{87}Sr/^{86}Sr$ measured | 2sigma_mean | $^{87}Sr/^{86}Sr_{initial}$ at 14.7 Ma | L (A) + R (B) model Age [Ma] | Ilt $^{87}Sr/^{86}Sr_{initial}$ | % | Ilt/Sme | % |
|---|---|---|---|---|---|---|---|---|---|---|---|---|---|---|
| GB 41 R, B[a] | Sme/altered Tuff | 18.9 | 2.4 | 7.875 | | | | | | | | | 11 | 19 (16) |
| GB37B L, A[a] | Sme/Tuff | 3.3 | 7.0 | 0.471 | 1.365 | 0.089 | 0.71160 | 0.000017 | | | | | | |
| GB37B R, A[a] | Sme/Tuff | 20 | <10 | | | | 0.71961 | 0.000016 | | | | | | |
| GB37B R, B[a] | Sme/Tuff | 22.6 | 3.8 | 5.947 | 17.234 | 1.120 | 0.71961 | 0.000016 | 0.71602 | 35.6 ± 5.0 | 0.71091 ± 21 | | | |
| GB35A L, A | Sme/Bentonite | <0.8 | <8 | | | | 0.71108 | 0.000026 | | | | | | |
| GB35A L, B | Sme/Bentonite | 0.3 | 27.8 | 0.011 | 0.031 | 0.002 | 0.71108 | 0.000026 | | | | | | |
| GB35A R, A | Sme/Bentonite | 0.3 | 0.9 | 0.333 | | 0.001 | | | | | | | | 8 (0) |

Sme = Smectite, L = leachate, R = residue, A = method A, B = method B.
[a]Discrete illite-rich samples.

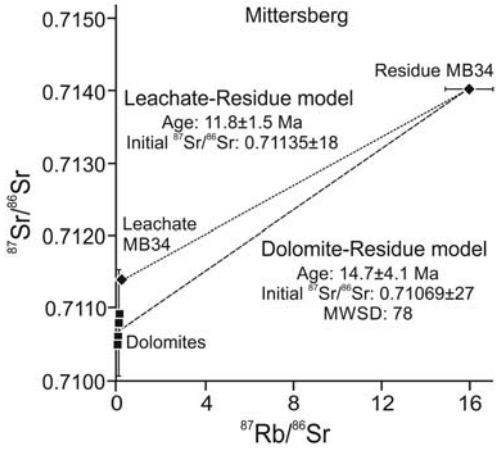


FIG. 9. Isochron plot of the Mittersberg deposits showing Rb-Sr data of dolomites (MB12, 18, 27 and 28) and smectite residue (MB34). The smectite leachate-residue pair is included for comparison. Squares: dolomite; diamonds: smectite from bentonite.

influenced by the included silicates or oxides included. They were used to compare a larger number of samples (Fig. 7a–f) on the basis of their $10^6$*(Sr/Ca) molar ratios, denoted hereafter as $Sr/Ca_m$, and Mn content, respectively. The $Sr/Ca_m$ and Mn contents measured by XRF are consistent with the ICP-MS results (Fig. 7a–f). Dolomites show negatively correlated $Sr/Ca_m$ and Mn content, while calcites display a positive but less distinct correlation of $Sr/Ca_m$ and Mn content. High $Sr/Ca_m$ of dolomites and calcites are related to high $\delta^{18}O$ values (Fig. 7c,d), whereas Mn contents and $\delta^{13}C$ values show a more complex relationship (Fig. 7e,f).

### *Rare earth element (*REE*) patterns*

The *REE* plus yttrium (*REE* + Y; Appendix 1, available from http://www.minersoc.org/pages/e_journals/dep_mat_cm.html) patterns (Fig. 8) were normalized against the post-Archaean Australian shale (PAAS, Nance & Taylor, 1976) as recommended by Bau & Möller (1992) for sedimentary environments. Both pedogenic and palustrine dolomites, as well as groundwater calcites show a slight enrichment of heavy *REE* ($LREE_{PAAS} \approx 0.5–0.1$ and $HREE_{PAAS} \approx 1.0–1.1$) indicating the remobilization of *HREE*, and complexation in carbonate-rich waters (Möller *et al*., 1984). The palustrine dolomites have small negative Ce and Eu anomalies suggesting slightly oxidizing conditions, and/or inheritance from the fluid phase interacting with detrital rocks. In contrast, the pedogenic dolomites and groundwater calcites display positive and negative Ce and Eu anomalies, suggesting variable redox conditions in soil and groundwater settings.

### *Chemical composition of smectites*

The chemical compositions of the smectite (<0.2 μm fraction) leachates and acid-treated residues of bentonites, tuffs and sandstone are shown in Tables 3 and 4. The first step (method A) of the 1 N and 6 N HCl treatment revealed that Ca and Mg are the main leachable elements with an average molar Mg/(Mg + Ca) ratio of 0.43 ± 0.11, consistent with previously reported exchangeable cation compositions (Grim & Güven, 1978; Ulbig, 1994). The leachates also contain Sr (7.0–90.1 μg/g), Rb (0.3–4.1 μg/g), as well as traces of As, Ba, Cu, Pb and V.

The smectite residues (method A) have small MgO (1.2–1.9 wt.%) and very small CaO contents (0.1 wt.%) which corresponds to a Mg/(Mg + Ca) molar ratio of 0.96–1.00 confirming the partial dissolution of the smectite octahedral sheet and possibly suggesting the presence of trace amounts of carbonate not detected by XRD or traces of residual Ca in the smectite interlayer. The acid treatment of residues released variable amounts of Fe (11.4–19.7 mg/g) but very little $SiO_2$ (<1.3 wt.%) indicating that tetrahedral sheets were only partially dissolved. Smectite residues from palustrine deposits (GB and MB) have an elevated Li content of ~20 μg/g (Table 3).

The 18 h acid treatment of smectite residues (method B) released Sr (1.0–3.7 μg/g) and Rb (7.8–22.6 μg/g). The Rb and K contents are positively correlated ($r^2 = 0.85$), suggesting that Rb is located in discrete illite or in the illite layers of the I-S. In both methods A and B, sample GB35A showed very small Sr and Rb contents. Sample GB35A has one of the smallest percentages of illite layers in I-S (Table 2) and was prone to clumping during treatment, possibly leading to an insufficient acid attack on the already small Sr and Rb contents in the illitic component.

The 'total' Sr contents of smectites (Leachate + Residue; mean = 29.4 ± 27.6 μg/g, 1 SD) exceed slightly the previous results (Vogt & Köster, 1978; mean: 19.5 ± 4.8 μg/g, 1 SD) of Na-exchanged smectites treated with 0.1 M EDTA and 0.1 N ammonium solution, probably because these treatments removed exchangeable Sr. The Sr content of the residues (mean: 2.7 ± 1.0 μg/g, 1 SD) is rather small. A

https://doi.org/10.1180/claymin.2017.052.2.01 Published online by Cambridge University Press

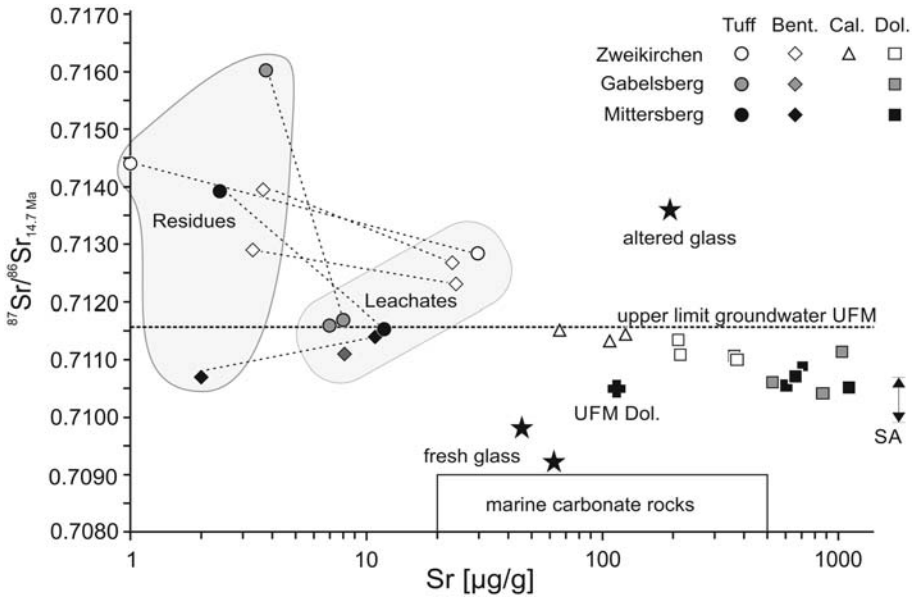


FIG. 10. Sr concentrations plotted *vs.*Sr isotope ratios at 14.7 Ma of carbonates and smectites, compared to previous studies in the North Alpine Foreland Basin. Thin, dashed lines connect smectite leachate-residue pairs. Stars: volcanic glass shards; black cross: dolomite in the UFM (Graup *et al*., 1981); SA: Sr isotope ratio range of Sandelzhausen fossil mammal teeth enamel (Tütken & Vennemann, 2009); box – Mesozoic marine carbonates (McArthur *et al.*, 2001; Zorlu, 2007; Geske *et al*., 2012). Upper limit of shallow (<150 m) groundwater in the UFM (~range 0.7080 to 0.712), according to data in Eichinger *et al.* (2007), Voerkelius *et al*. (2010) and Tütken *et al*. (2006).

'total' Rb content of 16.9 ± 5.5 µg/g (Leachate + Residue) was extracted, mostly located in the residues (14.4 ± 4.9 µg/g, 1 SD; Table 4). This is less than those reported by Vogt & Köster (1978; 31 ± 12 µg/g, 1 SD), indicating the partial extraction of Rb from smectite residues. Strontium is thus more easily extractable from absorbed and exchangeable positions (65 to 97%) whereas Rb is fixed more firmly in the residues (77 to 93%), similar to the results from the Clay Spur and Otay bentonites (Chaudhuri & Brookins, 1979).

### *Rb-Sr isotope results*

The Rb-Sr isotopic data reveal a systematic increase in the Rb/Sr ratio and $^{87}Sr/^{86}Sr$ and a decrease in Sr concentrations from dolomites *via* calcites to smectite leachates and residues (Table 4; Fig. 10). The lowest Rb/Sr ratio and $^{87}Sr/^{86}Sr$ are found in palustrine dolomites (0.005–0.013 and 0.71042–0.71113, respectively; Table 4) from Gabelsberg and Mittersberg, with slightly higher values in pedogenic dolomites from Zweikirchen (0.006–0.37 and 0.71105–0.71135, respectively; Table 4). Groundwater calcites from Zweikirchen have greater Rb/Sr ratios and $^{87}Sr/^{86}Sr$ (0.097–0.177 and 0.71138–0.71154, respectively) than the pedogenic dolomites from the same locality (Fig. 10; Table 4).

In the Gabelsberg and Mittersberg deposits, the Rb/Sr ratios (0.011–0.471) and $^{87}Sr/^{86}Sr$ (0.71108–0.71160) of the smectite leachates are greater than in the associated dolomites and were partly lower than the respective values of the smectite leachates from the Zweikirchen deposit (0.034–0.137, 0.71231–0.71285; Table 4). The Rb/Sr ratios (0.333–14.0) and $^{87}Sr/^{86}Sr$ (0.71401–0.72286) of the smectite residues are even higher and do not display systematic differences (Fig. 10). Illite-rich samples have the highest Rb/Sr ratios and $^{87}Sr/^{86}Sr$ values (Table 4).

The smectite leachate-residue pair model ages range from 11.8 to 35.5 Ma. Their initial $^{87}Sr/^{86}Sr$ values vary between 0.71091 and 0.72161 (Table 4). The largest initial $^{87}Sr/^{86}Sr$ values were determined in illite/mica-poor sample ZW50 with a low Rb/Sr ratio (2.108). The leachate-residue (L-R) pair ages (Table 4) are mostly older than the rhyolitic ash (14.7 ± 0.2 Ma; Abdul-Aziz *et al*., 2010), indicating the presence of

https://doi.org/10.1180/claymin.2017.052.2.01 Published online by Cambridge University Press

detrital illitic material in the <0.2 μm fractions (Table 2). Sample MB34 which does not contain detrital micaceous material yielded a L-R model age of 11.8 ± 1.5 Ma (Fig. 9). As all leachates from the separated clay fractions have more radiogenic Sr isotope ratios than the associated early diagenetic carbonates and as this Sr is located in an exchangeable position of the smectite, the isotope composition of the leachates may not be representative of the initial $^{87}Sr/^{86}Sr$ during smectite formation. We therefore determined an isochron age using early diagenetic palustrine dolomites and the smectite residue (<0.2 μm fraction) of a bentonite from Mittersberg (MB34) that does not contain detrital illitic components (Fig. 9). The calculated dolomite-smectite residue age of 14.7 ± 4.1 Ma is identical to the eruption age of the volcanic ash at 14.7 ± 0.2 Ma (Abdul-Aziz *et al.*, 2010) and its initial $^{87}Sr/^{86}Sr$ of 0.71069 (Table 4; Fig. 9) is identical to the average Sr isotope value (0.71070 based on values in Table 4) of palustrine dolomites.

## DISCUSSION

The geochemical data of dolomite, calcite and smectite in the Landshut bentonites provide some new insights into the fluid compositions and cation source(s) during carbonate formation and bentonitization in a terrestrial environment. Köster & Gilg (2015) suggested that the fluids responsible for carbonate formation and possibly bentonite formation of the Landshut bentonites were broadly similar to present-day Ca-Mg-$HCO_3^-$ groundwater in the UFM (molar Mg/Ca: 0.53–1.37; $CO_3^{2-}/Ca^{2+}$: 2.50–9.85, rarely ~25; Egger *et al.*, 1983). However, the unusual high Sr concentrations of bentonite-hosted dolomites (up to 1120 μg/g; Table 4) observed in the present study are difficult to reconcile with an unmodified freshwater composition (TDS: 0.28 g/L; Egger *et al.*, 1983). Sr-rich dolomites are often attributed to marginal marine lagoons, microbial-mediation or to strongly evaporative environments (*e.g.* Sánchez-Román *et al.*, 2011) where Sr content and $Sr/Ca_m$ correlate broadly with salinity (Banner, 1995). Marine or terrestrial evaporite deposits with sulfates or halides, however, are absent from the North Alpine Foreland Basin and the UFM was never subjected to marine incursions (Lemcke, 1973; Unger, 1996). Sr-rich carbonate formation in saline environments during the Mid-Miocene has rarely been reported in the North Alpine Foreland Basin. The alkaline-saline lake in the Mid-Miocene Ries impact crater (Arp & Wiesheu, 1997) and calcitic saline soils with minor dolomite and palygorskite at Mergelstetten (Kallis *et al.*, 2000) are notable exceptions in terms of the formation of carbonates with >2000 μg/g Sr. Evaporation processes, as expected in a palustrine setting, might, therefore, have played a significant role for dolomite formation in the Landshut bentonites.

### *Salinity and Mg/Ca of the dolomite and calcite-forming water*

The correlation of $Sr/Ca_m$ with the $\delta^{18}O$ values of the dolomites ($r^2 = 0.84$; Fig. 7c,d) indicates evaporation (Gasse *et al.*, 1987; Banner, 1995) and suggests that the salinity of the water that precipitated dolomites is also correlated with $Sr/Ca_m$ and Sr content (Folk & Land, 1975; Banner, 1995). The presence of Li only in Sr-rich palustrine dolomites (13–20 μg/g; Table 3) also implies elevated salinities (Gaines, 1980). The dolomites in the Landshut bentonites have Sr concentrations rather similar to those of carbonates from fresh to brackish lakes in the Palaeogene Madrid basin (202–496 μg/g Sr, $Sr/Ca_m$: 250–640; Bustillo *et al.*, 2002), the Miocene La Roda 'white earths' (494–834 μg/g Sr, $Sr/Ca_m$: 1000–1500; García del Cura *et al.*, 2001), both in Spain, or the Holocene lake sediments of the northern Sahara (1033–3246 μg/g Sr, $Sr/Ca_m$: 1640–5580; Gasse *et al.*, 1987).

The $Sr/Ca_m$ of dolomite and calcite in the Landshut bentonites may be derived from those of shallow groundwater in the UFM (Wagner *et al.*, 2003; Eichinger *et al.*, 2007; Kainzmaier *et al.*, 2007) using established Henderson and Kracek distribution factors for calcite (0.03 ± 0.2, Banner, 1995), non-stoichiometric dolomite ($D_{Sr} = 0.0118 + \Delta Ca^*$ 0.0039), and a high $D_{Sr}$ of 0.051 for palustrine dolomite (Vahrenkamp & Swart, 1990), taking rapid precipitation and evaporation into account (Gaines, 1980; Lorens, 1981; Banner, 1995). Therefore, a Sr-rich precursor phase such as Sr-rich aragonite (Tucker & Wright, 1990; Anadón *et al.*, 2002) in the form of Charophyta remains in palustrine dolomite (Köster & Gilg, 2015) is not required. Moreover, most Charophyta species are composed of calcite (Tucker & Wright, 1990) and residual aragonite or its dissolution fabric has never been observed in bentonites (Vogt, 1980; Köster & Gilg, 2015). In addition, bioclast-bearing (Gabelsberg) and bioclast-poor dolomites (Mittersberg) have identical Sr concentrations and $^{87}Sr/^{86}Sr$ (Table 4; Fig. 10) indicating the same Sr sources.

Sánchez-Román *et al.* (2011) recently reported high Nernst and Henderson and Kracek Sr partition coefficients (22–37 and 0.12–0.22, respectively) for microbially mediated dolomites. Dolomicritic grains

https://doi.org/10.1180/claymin.2017.052.2.01 Published online by Cambridge University Press

TABLE 5. $10^6$*(Sr/Ca) ratios of calcites and dolomites, and salinities derived using a freshwater salinity of 0.28 g/L for waters precipitating calcite (from Egger *et al*., 1983).

| | Median $10^6$*(Sr/Ca) molar | Mean | Min | Max | Median SAL (g/L) | Mean |
|---|---|---|---|---|---|---|
| Pedogenic calcite | 81 | 78 | 27 | 128 | 0.28 | 0.28 |
| Groundwater calcite | 83 | 88 | 9 | 224 | 0.28 | 0.28 |
| Palustrine dolomite | 1,513 | 1,837 | 894 | 4,379 | 5.30 | 6.43 |
| Pedogenic dolomite | 534 | 651 | 435 | 1.042 | 1.87 | 2.28 |

and aggregates resembling microbial remains were observed in the Landshut bentonites (Köster & Gilg, 2015). The low cation ordering $d_{015}/d_{110}$ ratios of dolomite, its non-stoichiometric composition, and the presence of framboidal pyrite in bluish bentonite (Figs 2 and 4b; Ulbig, 1994) that could be related to bacterial sulfate reduction (e.g. van Lith *et al.*, 2003) might be suggestive of microbial mediation for dolomite formation. Nonetheless, dolomicrite also forms by rapid inorganic precipitation (Banner, 1995). Assuming that microbial activity occurred in palaeosols of the UFM (Schmid, 2002) and was probably beneficial for dolomite formation (*e.g.* Sánchez-Román *et al*., 2011), it is still considered a minor factor for the observed Sr enrichment in the palustrine dolomites. This is because the $\delta^{13}C$ values ($-7.3 \pm 0.3$ ‰, 1 SD; Köster & Gilg, 2015) of dolomites are inconsistent with typical organic derived microbial carbon isotope values, being too low for fermentation processes but too high for sulfate reduction (Nelson & Smith, 1996) to explain oxygen isotope enrichments.

Assuming a starting salinity (TDS) of 0.28 g/L in water (Egger *et al*., 1983), a $Sr/Ca_m$ of ~80 (Wagner *et al*., 2003) for calcite-precipitating water (Table 5) and a linear relationship of salinity with $Sr/Ca_m$, we calculated salinities of 2.3 to 6.4 g/L during dolomite precipitation, with extreme values of 15.3 g/L in palustrine settings (Table 5) most affected by evaporation. These salinities are consistent with dolomite formation in lacustrine environments and in the range of dolomite-precipitating brackish waters of Lake Balaton (0.5 g/L; higher during playa-like periods), Lake Neusiedl (1.5 g/L), and Lake Specchio di Venere (16.0 g/L) (Last, 1990).

As both the molar Mg/Ca and the salinity of the fluid exert a major control on dolomite precipitated from it (Folk & Land, 1975) even in non-evaporite-bearing environments (Last, 1990), the results obtained can be used to estimate the molar Mg/Ca of the dolomite precipitating water, using the Mg/Ca–salinity relationship of Folk & Land (1975). A molar Mg/Ca of 2–5 was derived, assuming that the influence of temperature, alkalinity or pH is either negligible or constant. The molar Mg/Ca is consistent with dolomite-forming lacustrine environments such as Lake Balaton during dry periods (1.5–3.5; Tompa *et al*., 2014) and water in its sediment pore-space (7–12; Müller *et al*., 1972), and water of Lake Neusiedl (7.9; Schroll & Wieden, 1960), suggesting that our Mg/Ca estimates are realistic. The molar Mg/Ca of 2 to 5 for dolomite precipitating water is also consistent with the calcium-rich composition of dolomites (Folk & Land, 1975).

The molar Mg/Ca of water in pedogenic and groundwater settings precipitating calcite was determined using a linear temperature-dependant relationship which relates the Mg/Ca of calcite to that of the water from which it formed (Last, 1980). In addition, the salinity–Mg/Ca diagram of Folk & Land (1975) was used to estimate the Mg/Ca of calcite precipitating water. These two methods yield molar Mg/Ca of 0.8–1.8 at 15–31°C (Köster & Gilg, 2015) and of 1.0 respectively. Both results are consistent with the Mg/Ca of waters in the UFM (range 0.53–1.37; Egger *et al*., 1983), indicating that the calcites in bentonites precipitated from largely unmodified soil and groundwater.

### *Redox–sensitive elements*

Dolomites and calcites from oxidized, intermediate and reduced bentonites (Figs 2 and 3) have highly contrasting Mn concentrations with calcites generally being enriched in Mn relative to dolomites (Table 3). The contrasting compositions of calcites and dolomites suggests distinct fluid compositions, as the preferential inclusion of Mn into Mg sites would have produce rather Mn-enriched dolomite (Kretz, 1982) if they had formed from the same fluid.

https://doi.org/10.1180/claymin.2017.052.2.01 Published online by Cambridge University Press

Pyrite-bearing blue bentonites from the Zweikirchen deposit contain groundwater calcites that are highly enriched in Mn (2880–4720 μg/g) but have low U concentrations (Table 3). As $Mn^{2+}$ is water-soluble in reducing environments whereas uranium is not, calcites will be enriched in $Mn^{2+}$ if precipitated from such water but will incorporate little uranium. The composition of the calcites therefore indicates reducing conditions and/or a high Mn availability, and possibly slow precipitation rates (Dromgoole & Walter, 1990; Rimstidt *et al*., 1998), as suggested by low $\delta^{13}C$ values (Fig. 7e,f) and redox limits (~200 μg/g Mn) defined by Lohmann (1988). However, the large range of Mn concentrations (37–4839 μg/g) in calcites examined by p-XRF (Fig. 7a–f; Appendix 2, http://www.minersoc.org/pages/e_journals/dep_mat_cm.html) suggests highly variable redox conditions during calcite formation in bentonites, as was indicated by variable *REE*+Y patterns (Fig. 8b) and contrasting Ce anomalies, with negative Ce anomalies indicating less reducing to oxidizing conditions (Möller *et al*., 1984; Bau & Möller, 1992). The presence of Mn-poor calcite-spar (Appendix 2, available from http://www.minersoc.org/pages/e_journals/dep_mat_cm.html; Fig. 4d) in grey-brown bentonite from Hader (31–282 μg/g; Fig. 3) and calcites with high and low Mn concentrations in yellow bentonites of Gabelsberg and Zweikirchen (Appendix 2, available from http://www.minersoc.org/pages/e_journals/dep_mat_cm.html, Fig. 2) confirms later oxidation because Mn-rich calcites cannot form simultaneously with oxidized (yellow) bentonite. So, although Mn-rich calcites in pyrite-bearing blue bentonites are indicative of some cogenetic calcite and bentonite formation in reducing waters, Mn-rich and Mn-poor calcites in oxidized bentonites require contrasting redox conditions for their formation (Lohmann, 1988; Tucker & Wright, 1990), and indicate at least two calcite generations.

The down-section increasing Mn concentrations (353–1,700 μg/g; Table 3) in pedogenic dolomites of the Zweikirchen deposit point to increasingly reducing conditions and higher Mn availability in soils with depth, in accordance with positive Ce anomalies and *REE* + Y patterns (Fig. 8b). Note that groundwater calcites in the lower parts of the Zweikirchen deposit have even higher Mn concentrations (2,880–4,720 μg/g) than pedogenic dolomites (Möller *et al*., 1984; Bau & Möller, 1992) at the same locality, consistent with increasingly reducing conditions with depth.

Palustrine dolomite has the lowest Mn concentrations (305–580 μg/g; Table 3) and show less pronounced (MB) or absent (GB) downward trends in Mn content. The Mn concentrations and low $\delta^{13}C$ values of the palustrine dolomites (−7.3 ± 0.3‰, 1 SD; Köster & Gilg, 2015) are similar to lacustrine La Roda "white earths" formed in oxic to suboxic environments (García del Cura *et al*., 2001). The systematically negative Ce anomalies (Fig. 8a) and high U concentrations (2.3–13.6 μg/g; Table 3) thus point to rather oxidizing conditions during dolomite precipitation.

### *Sr provenance for carbonates*

Dolomites, calcites and the smectite leachates all have very small Rb/Sr ratios; therefore the measured $^{87}Sr/^{86}Sr$ values (Table 4) do not require any age corrections. The $^{87}Sr/^{86}Sr$ of the Sr-rich palustrine dolomites from the two studied deposits ~12 km apart are very homogeneous (0.71052–0.71113) and only slightly less radiogenic than the pedogenic dolomites from the Zweikirchen deposit (0.71105–0.71135). Both are significantly more radiogenic than the unaltered volcanic glasses (~0.7098) at 14.7 Ma that contain only 40 μg/g Sr (Horn *et al*., 1985) and therefore indicate that Sr and, by inference, also Ca and Mg were not derived from volcanic glasses but introduced from the surrounding sedimentary environment. The Sr isotope values of our dolomites are similar to those of early diagenetic dolomite unrelated to bentonite in the UFM (Horn *et al*., 1985) and mammal tooth enamel from the Sandelzhausen fossil site, situated 3.5 km north (Fig. 1) of Mittersberg (Tütken & Vennemann, 2009). The Sr isotopic compositions of the UFM dolomite and fossil tooth were interpreted by Graup *et al*. (1981) and by Tütken & Vennemann (2009) as representative of Miocene surface sediments and waters.

The $^{87}Sr/^{86}Sr$ of the Sr-poor groundwater calcites at the Zweikirchen deposit are, however, more radiogenic than the pedogenic dolomites from the same site (Fig. 10). This indicates that two distinct fluids were involved in the precipitation of the two carbonate minerals at this site in support of the conclusions from Sr and Mn trace-element chemical data.

The dolomites and calcites also reveal co-varying $^{87}Sr/^{86}Sr$, Sr concentrations, and $\delta^{18}O$ values (Fig. 11). This emphasizes contrasting Sr sources and also suggests two end-members: a generally Sr-rich brackish surface water with low $^{87}Sr/^{86}Sr$, similar to the ratios in palustrine dolomites (with a mean of ~0.71070 derived from Table 4) and a dilute groundwater with more radiogenic Sr and $^{87}Sr/^{86}Sr$ greater than or equal to those of calcites (≥0.71150

https://doi.org/10.1180/claymin.2017.052.2.01 Published online by Cambridge University Press

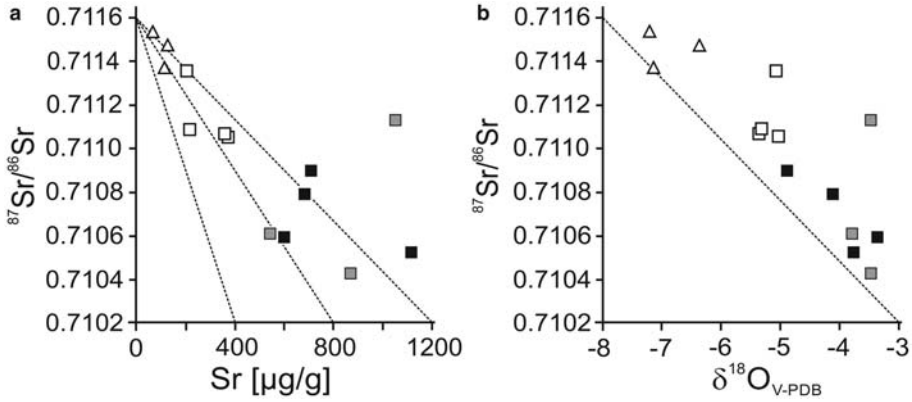


FIG. 11. Covariance of $^{87}Sr/^{86}Sr$ with: (a) Sr concentration; and (b) $\delta^{18}O$ values (from Köster & Gilg, 2015). Triangles (white): calcite, squares: pedogenic (white); and palustrine dolomite (grey and black).

derived from the values Table 4). The Sr isotope values of dolomites and calcites in bentonites are within the $^{87}Sr/^{86}Sr$ range for sediments and groundwaters of the UFM in the North Alpine Foreland Basin (0.708–0.713; Tütken *et al*., 2006; Eichinger *et al*., 2007; Voerkelius *et al*., 2010; Waber *et al*., 2014) and consistent with the high $^{87}Sr/^{86}Sr$ values (>0.710) of sediments in the Eastern Molasse basin (Tütken & Vennemann, 2009). Here, the $^{87}Sr/^{86}Sr$ values of waters in the UFM mirror the composition of the sediments, with Sr having high $^{87}Sr/^{86}Sr$ derived from silicate rocks of the Variscan basement (crystalline basement rocks of the Ries impact: 0.7100–0.7180 and 0.7216–0.7236 in Graup *et al*., 1981; Horn *et al*., 1985; plutonic rocks of the Bavarian Forest: 0.70881–0.74060; Siebel *et al*., 2005; Köhler *et al*., 2008) and Sr with low $^{87}Sr/^{86}Sr$ derived from lime- and dolostones of the Mesozoic cover both in Alps and the South German Block (0.70835 to 0.70965; McArthur *et al*., 2001; Zorlu, 2007; Geske *et al*., 2012).

High weathering rates of lime- and dolostone clasts in soils profoundly affect the Sr isotopic composition of water even in silicate-rich sediments (Blum *et al*., 1998) because of the prevailing release of Sr from carbonates (Clow *et al*., 1997). The widespread dissolution and precipitation of carbonates in sediments (Egger *et al*., 1983) and paleosols of the UFM (Schmid, 2002) are therefore responsible for both the formation of Ca-Mg-$HCO_3$ waters (Egger *et al*., 1983) and a disparate release of Sr from carbonate weathering in the UFM. The rapid weathering of dolomite in soils is also a major Mg source that can produce waters with high molar Mg/Ca ratios (~2.0) in dolomite-bearing, mixed carbonate-siliciclastic sediments (Jin *et al*., 2008). Therefore the low $^{87}Sr/^{86}Sr$ (~0.71070) in the dolomites of this study argue for Sr predominantly but not exclusively derived from lime- and dolostones whereas the higher $^{87}Sr/^{86}Sr$ (~0.71150) of calcites point to more radiogenic Sr from silicate weathering, as confirmed by high Mn and Rb contents (Tables 3 and 4), and high Rb/Sr (Table 4). The latter point to Rb/Sr of groundwater in carbonate-free, siliciclastic sediments of the UFM (carbonate-free: 0.0266; carbonate-bearing: 0.0023 and 0.0025, Wagner *et al*., 2003; Kainzmaier *et al*., 2007).

### *Sr isotope geochemistry of smectites and carbonates, and Rb-Sr dating*

Although the Sr content in smectites (<0.2 µm fractions) is mostly concentrated in the exchangeable interlayer and is much smaller than in the associated carbonates, the $^{87}Sr/^{86}Sr$ values are much larger (Fig. 10, Table 4) than those of the soil and groundwater carbonates (Fig. 4a,c,d). This suggests strongly that the interlayer Sr in the smectites has been partly or completely exchanged after carbonate formation with more radiogenic fluids than those involved in carbonate precipitation.

This post-formational interlayer exchange is corroborated by a comparison of the molar Mg/Ca (MB and GB: 0.59 ± 0.21; ZW: 1.15 ± 0.21) in the exchangeable interlayer site with the Mg/Ca (2–5) estimated for the dolomite precipitating fluid, assuming a cogenetic origin of dolomite and bentonite (Köster & Gilg, 2015). The molar Mg/Ca ratios of the smectite leachates (<0.2 µm fractions) are in equilibrium with

https://doi.org/10.1180/claymin.2017.052.2.01 Published online by Cambridge University Press

a water having a molar Mg/Ca ratio of 0.9–1.5. These values are lower than the Mg/Ca values (2–5) estimated for the fluid involved in dolomite formation even taking into account preferential Ca uptake into the smectite interlayer (Laudelout *et al.*, 1968; Sayles & Mangelsdorf, 1979), and are more like values (0.8–1.8) estimated for the water(s) that precipitated calcite. The chemical (Sr, Mg, Ca) and isotopic ($^{87}Sr/^{86}Sr$) compositions of smectite leachates are therefore not indicative of the fluids involved in bentonite formation, nor are they related to dolomite precipitation in bentonites.

The post-formational interlayer cation exchange with more radiogenic Sr has influence on the smectite leachate-residue model ages of the <0.2 μm fractions which should be yielding younger apparent ages. Nevertheless almost all <0.2 μm fractions reveal smectite leachate–residue ages (35.5–17.5 Ma; Table 4) in excess of the depositional age of the volcanic ash (14.7 Ma ± 0.2 Ma, Abdul-Aziz *et al.*, 2010). Therefore, an illitic component consisting of discrete illite and/or R0 I-S (Tables 1 and 2; Fig. 5) is probably responsible for the high Rb/Sr in the smectite residues (2.1 to 14.0; Table 4) and also the excess ages. Potential contaminants are detrital sedimentary clays in the UFM or fine fractions of shales and limestones from the base of the Northern Calcareous Alps that have high $^{87}Sr/^{86}Sr_{14.7\ Ma}$ and Rb/Sr values (Kralik, 1983; Horn *et al.*, 1985).

However, a single bentonite sample (MB34) from the Mittersberg deposit (Figs 1 and 2) not containing detrital illitic components is characterized by the absence of discrete illite and a small amount of illite layers (<10%) in mixed-layer I-S (Table 2; Fig. 5). Both smectite leachate-residue (11.8 ± 1.5 Ma) and dolomite-residue models (14.7 ± 4.1 Ma) indicate an age (Fig. 9; Table 4) which post-dates ash deposition.

This illite-poor I-S in sample MB 34 and possibly also in samples containing older detrital illitic components could have been formed by illitization of smectite during wetting and drying cycles in the palustrine environment (*e.g.* Eberl *et al.*, 1986; Hugget & Cuadros, 2005) or even directly from the volcanic glass (Gilg *et al.*, 2003). The syngenetic dolomite-smectite age model and the elevated Li concentrations in both the palustrine dolomites and the smectite residues (~20 μg/g; Table 3) indicate a cogenetic formation from Li-bearing evaporated fluids, and thus an onset of bentonitization during dolomite formation. The Rb-Sr data (Fig. 9) also suggest that bentonitization of the volcanic ash in the Landshut bentonites occurred no later than 4 m.y. after deposition.

## BENTONITE AND CARBONATE FORMATION

Two modes are proposed here to explain dolomite and calcite formation in the Landshut bentonites, as well as the onset of bentonitization (Fig. 12). Although these modes may resemble features of topographic "highs" and "lows" suggested by Ulbig (1994, 1999), they are based on the fluvial-lacustrine depositional environment of the anastomosing to braided river system and associated palaeosols of the UFM (Schmid, 2002; Maurer & Buchner, 2007). This circumvents the problematic preservation of unconsolidated volcanic ash on topographic "highs" (Ulbig, 1994) in a strongly seasonal climate and the inherent dryness of such topographic "highs" (Böhme *et al.*, 2007) that contradicts the sedimentological evidence of moist soils and wetlands (Unger, 1996; Schmid, 2002; Maurer & Buchner, 2007; Abdul-Aziz *et al.*, 2010).

### *Palustrine settings*

(1) Palustrine deposits, such as Mittersberg and Gabelsberg, have a pronounced asymmetric character with tuff and/or dolomite in the upper part but bentonite with or without carbonates in the lower part above a clayey footwall (Fig. 12). Deep-reaching root features in partially altered tuffs and bentonites, and modern rooting depths (Canadell *et al.*, 1996) of sclerophyllous (5.2 ± 0.8 m), tropical (7.3 ± 2.8 m) and temperate deciduous forest and shrubland (2.9 ± 0.9 m) resembling Miocene vegetation (Böhme *et al.*, 2007) imply strict surface vicinity of the bentonite deposits during the onset of bentonite and carbonate formation. The elevated Li concentrations (~20 μg/g; Table 3) and Sr isotope data of smectite residue (especially MB34; Table 4; Fig. 9) and palustrine dolomites strongly suggest a cogenetic origin from the same evaporated Li-enriched fluid with low $^{87}Sr/^{86}Sr$ (~0.71070), and thus links smectite to dolomite formation. The formation of dolomite and bentonite in floodplains, ponds or wetlands therefore occurred in brackish evaporated surface waters with a molar Mg/Ca of 2 to 5, but a fluid with a more radiogenic Sr isotope composition (Fig. 10) was later involved in cation exchange reactions. A combination of insufficient leaching of K from the $K_2O$-rich glass (Ulbig, 1994) due to frequent wet-dry cycles (Eberl *et al.*, 1986, 1993) and cyclic water-logging in palustrine deposits (Köster & Gilg, 2015) favouring a return to reducing conditions could have led to the incipient illitization of smectite and formation of illite-poor R0

https://doi.org/10.1180/claymin.2017.052.2.01 Published online by Cambridge University Press

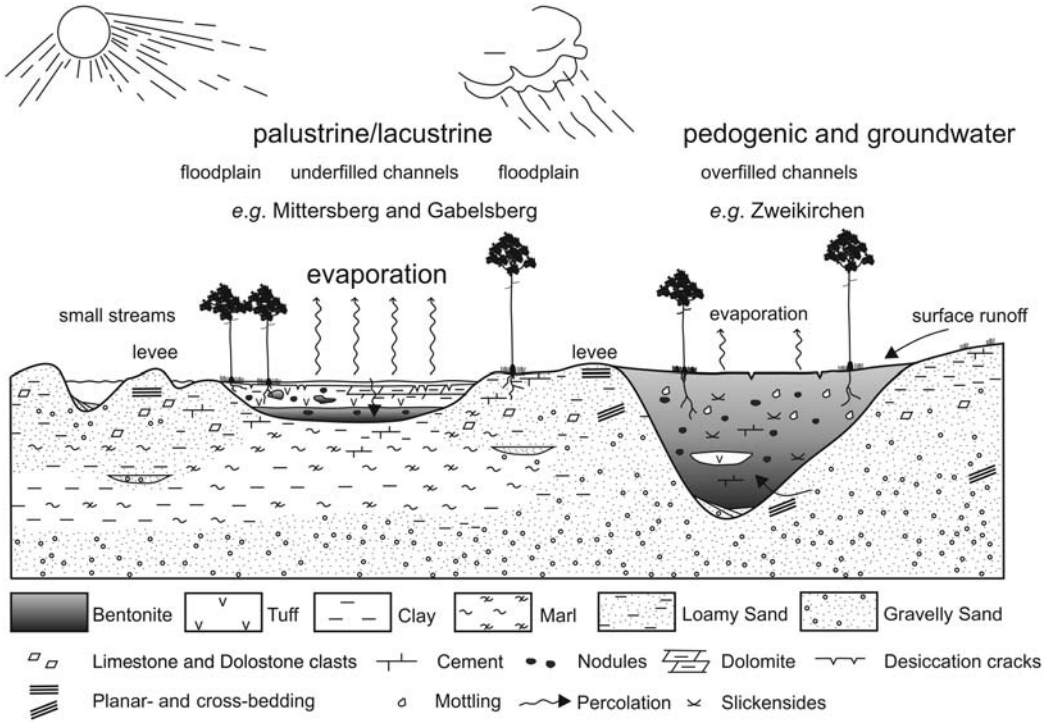


FIG. 12. Dolomite and calcite formation in bentonites in the alteration and depositional context of the fluviatile-lacustrine environment of the UFM. Not drawn to scale!

I-S, similar to observations in calcareous palaeosols of the UFM (Stanjek & Marchel, 2008), although the direct formation of illite-poor R0 illite-smectite from the K-rich glass cannot be excluded. Bentonitization was therefore limited to phreatic horizons permanently saturated with brackish, Sr-rich and Li-bearing water and probably isolated against dilute groundwater having more radiogenic Sr by the clayey footwalls (Fig. 2).

### *Pedogenic and groundwater-dominated settings*

(2) Pedogenic- and groundwater-dominated deposits (Fig. 12), such as that at Zweikirchen, have the characteristic symmetry of bentonite–tuff–bentonite (Vogt, 1980) hosted by sand or gravel. It is suggested that this is the result of its more protected alteration setting (Fig. 12) that has less evaporation and less risk of desiccation to dryness as the palustrine environments, indicated by lower $\delta^{13}C$ and $\delta^{18}O$ values (Fig. 7; and Köster & Gilg, 2015), lower Sr concentrations but higher Mn and Rb/Sr and $^{87}Sr/^{86}Sr$ ratios (Tables 3, 4, Fig. 10). Dolomite and calcite are abundant but calcites dominate the lower horizons. The lower parts of the deposits (Figs 2 and 12) were continuously below reducing groundwater levels while water levels fluctuated at the top (Köster & Gilg, 2015). Infiltration of surface water and significant evaporation (Fig. 12) were nevertheless essential for the precipitation of dolomite. In contrast, calcite formation and bentonitization occurred in the predominantly saturated zone from waters similar to recent reducing groundwater in the UFM. Some Mn-poor calcites (Table 3) formed during later oxidation events in the now yellow bentonite, possibly from the same waters that were involved in post-formational cation exchange reactions with the smectite interlayer (Fig. 10).

## SUMMARY

The major and trace-element geochemistry including Sr isotopes of carbonates and smectites from the terrestrial Landshut bentonites in Germany were examined systematically to explore fluid composition and cation provenance, and reveal clearly that two distinct fluids were involved in dolomite and calcite formation.

https://doi.org/10.1180/claymin.2017.052.2.01 Published online by Cambridge University Press

Strontium, Ca and Mg for carbonate and bentonite formation were re-mobilized by carbonate and silicate weathering in soils and from subsurface sediments in the North Alpine Foreland Basin.

Dolomites precipitated from evaporated surface water with variable salinity and high molar Mg/Ca. Calcite formation was restricted to dilute, both oxidizing and reducing ground- and soil waters with low molar Mg/Ca. Dolomite-rich palustrine environments received a larger contribution of Sr from lime- and dolostone weathering, whereas pedogenic and groundwater settings are characterized by more radiogenic Sr from silicate weathering.

The original interlayer cation composition in all smectites appears not to be fully preserved and was, at least partly, replaced with cations from more radiogenic, younger groundwater.

Most <0.2 μm fractions separated from bentonites still contain detrital illitic components. However, a <0.2 μm fraction of the bentonite (MB34) from Mittersberg that contains no detrital illitic material has been dated at 14.7 ± 4.1 Ma using the Rb-Sr method on the acid-leached <0.2 μm fraction and cogenetic dolomites. The smectite-rich <0.2 μm fraction of the Mittersberg bentonite contains some illitic components as an interstratified clay mineral that probably formed during pedogenesis in a palustrine environment, and/or directly from the alteration of a K-rich volcanic glass. The geochronological data show that the bentonitization of volcanic ash in the terrestrial distal Landshut bentonites occurred within <4 million years. The Rb-Sr method therefore appears to be a new viable technique for dating smectites and associated carbonates from terrestrial bentonites using acid-leach techniques, possibly even in combination with K-Ar dating.

## ACKNOWLEDGEMENTS

This publication is part of the doctoral thesis of the first author at the Lehrstuhl für Ingenieurgeologie, Technische Universität München, Germany supervised by Prof. Dr H. Albert Gilg. Prof. Dr Stefan Hölzl is acknowledged for access to, and help with and advice about Sr isotope analyses in the ZERIN-lab at the Ries Crater Museum Nördlingen. Dr Jürgen Bär at the Institut für Werkstoffkunde, Universität der Bundeswehr München, supported the authors in terms of access to the field-emission scanning electron microscopy facility. The ICP-MS analyses of method B were determined by Dr Klaus Simon at the Institut für Geochemie, Georg-August-Universität Göttingen. The authors are also grateful for access to bentonite mines granted by Bernhard Ratzke, Süd-Chemie AG (now Clariant), and the cooperation of Ulrich Boehnke, S&B Industrial Minerals (now Imerys). Finally, the authors are very grateful for the efforts of the reviewers Javier Cuadros and Helge Stanjek, whose comments improved the manuscript considerably, and the useful remarks of the editor. The C, O and Sr isotope, and geochemical analyses were supported financially by a Society of Economic Geologists SEG Graduate Fellowship Award 2012.

## REFERENCES

Abdul-Aziz H., Böhme M., Rocholl A., Zwing A., Prieto J., Wijbrans J.R., Heissig K. & Bachtadse V. (2010) Integrated stratigraphy and $^{40}Ar/^{39}Ar$ chronology of the Early to Middle Miocene Upper Freshwater Molasse. *International Journal of Earth Sciences*, **97**, 115–134.

Anadón P., Utrilla R. & Vázquez A. (2002) Mineralogy and Sr–Mg geochemistry of charophyte carbonates: a new tool for paleolimnological research. *Earth and Planetary Science Letters*, **197**, 205–214.

Arp G. & Wiesheu R. (1997) Ein kontinuierliches Profil von Algenbiohermen bis zu Seetonen des miozänen Rieskratersees: sequenzen, Mikrofazies und Dolomitisierung. *Geologische Blätter für Nordost-Bayern*, **47**, 461–486.

Banner J.L. (1995) Application of the trace element and isotope geochemistry of strontium to studies of carbonate diagenesis. *Sedimentology*, **42**, 805–824.

Bau M. & Möller P. (1992) Rare earth element fractionation in metamorphogenic hydrothermal calcite, magnesite and siderite. *Mineralogy and Petrology*, **45**, 231–246.

Blum J.D., Gazis C.A., Jacobsen A.D. & Chamberlain C.P. (1998) Carbonate *vs.* silicate weathering in the Raikhot watershed within the High Himalayan crystalline series. *Geology*, **26**, 411–414.

Böhme M., Bruch A.A. & Selmeier A. (2007) The reconstruction of Early and Middle Miocene climate and vegetation in southern Germany as determined from the fossil wood fauna. *Palaeogeography, Palaeoclimatology, Palaeoecology*, **253**, 91–114.

Budd D.A. (1997) Cenozoic dolomites of carbonate islands: their attributes and origin. *Earth-Science Reviews*, **42**, l–47.

Bustillo M.A., Arribas M.E. & Bustillo M. (2002) Dolomitization and silicification in low-energy lacustrine carbonates (Paleogene, Madrid Basin, Spain). *Sedimentary Geology*, **151**, 107–126.

Canadell J., Jackson R.B., Ehleringer J.R., Mooney H.A., Sala O.E. & Schulze E.-D. (1996) Maximum rooting depth of vegetation types at the global scale. *Oecologia*, **108**, 583–595.

Casado A.I., Alonso-Zarza A.M. & La Iglesia Á. (2014) Morphology and origin of dolomite in paleosols and lacustrine sequences. Examples from the

https://doi.org/10.1180/claymin.2017.052.2.01 Published online by Cambridge University Press

Miocene of the Madrid Basin. *Sedimentary Geology*, **312**, 50–62.

Chaudhuri S. & Brookins D.G. (1979) The Rb-Sr systematics in acid-leached clay minerals. *Chemical Geology*, **24**, 231–242.

Clauer N. (1979) Relationship between the isotopic composition of strontium in newly formed continental clay minerals and their source material. *Chemical Geology*, **27**, 115–124.

Clauer N., Hoffert M. & Karpoff A.-M. (1982) The Rb-Sr isotope system as an index of origin and diagenetic evolution of southern Pacific red clays. *Geochimica et Cosmochimica Acta*, **46**, 2659–2664.

Cleveland G.B. (1960) Geology of the Otay bentonite deposits, San Diego County, California. *California Division of Mines*, Special Report, 64, 16 pp.

Clow D.W., Mast M.A., Bullen T.D. & Turk J.T. (1997) Strontium 87/strontium 86 as a tracer of mineral weathering reactions and calcium sources in an alpine/subalpine watershed, Loch Vale, Colorado. *Water Resources Research*, **33**, 1335–1351.

Decher A., Bechtel A., Echle W., Friedrich G. & Hoernes S. (1996) Stable isotope geochemistry of bentonites from the island of Milos (Greece). *Chemical Geology*, **129**, 101–113.

Delgado A. (1993) *Estudio isotópico de los procesos diagenéticos e hidrotermales relacionados con la génesis de bentonitas (Cabo de Gata, Almería)*. Thesis doctoral, Universidad de Granada, España, 410 p.

Delgado A. & Reyes E. (1993) Isotopic study of the diagenetic and hydrothermal origins of the bentonite deposits at Los Escullos (Almería, Spain). Pp. 675–678 in: *Current Research in Geology Applied to Ore Deposits* (P. Fenoll Hach-Ali, J. Torres-Ruiz & F. Gervilla, editors). University of Granada, Spain.

Dromgoole E. & Walter L. (1990) Iron and manganese incorporation into calcite: effects of growth kinetics, temperature and solution chemistry. *Chemical Geology*, **81**, 311–336.

Eberl D.D., Środoń J. & Northrop H.R. (1986) Potassium fixation in smectite by wetting and drying. Pp. 296–326 in: *Geochemical Processes at Mineral Surfaces* (J.A. Davis & K.F. Hayes, editors). American Chemical Society Symposium Series, 323, American Chemical Society, Washington, D.C.

Eberl D.D., Velde B. & McCormick T. (1993) Synthesis of illite-smectite from smectite at Earth surface temperatures and high pH. *Clay Minerals*, **28**, 49–60.

Egger R., Eichinger L., Rauert W. & Stichler W. (1983) Untersuchung zum Grundwasserhaushalt des Tiefenwassers der Oberen Süßwassermolasse durch Grundwasseraltersbestimmung. *Informationsberichte Bayerisches Landesamt für Wasserwirtschaft*, **8/83**, 99–145.

Eichinger L., Lorenz G. & Heidinger M. (2007) Bohrung Uetlibergtunnel: interpretation der isotopenhydrologischen, hydrochemischen und gasphysikalischen Untersuchungsergebnisse. *Nagra Arbeitsbericht*, **NAB 07–08**, 1–59.

Folk R.L. & Land L.S. (1975) Mg/Ca ratio and salinity: two controls over crystallization of dolomite. *American Association of Petroleum Geologists Bulletin*, **59**, 60–68.

Freudenberger W. & Schwerd K. (1996) *Erläuterungen zur Geologischen Karte von Bayern 1:500000*. Bayerisches Geologisches Landesamt, Germany, 329 pp.

Frisch W., Kuhlemann J., Dunkl I., & Brügel A. (1998) Palinspastic reconstruction and topographic evolution of the Eastern Alps during late Tertiary tectonic extrusion. *Tectonophysics*, **297**, 1–15.

Gaines A.M. (1980) Dolomitization kinetics: recent experimental studies. *SEPM Special Publication*, **28**, 81–86.

Gao X., Wang P., Li D., Peng Q., Wang C. & Ma H. (2012) Petrologic characteristics and genesis of dolostone from the Campanian of the SK-I Well Core in the Songliao Basin, China. *Geoscience Frontiers*, **3**, 669–680.

García del Cura M.A., Calvo J.P., Ordonez S., Jones B.F. & Canaveras J.C. (2001) Petrographic and geochemical evidence for the formation of primary, bacterially induced lacustrine dolomite: La Roda 'white earth' (Pliocene, Central Spain). *Sedimentology*, **48**, 897–915.

Gasse F., Fontes J.C., Plaziat J.C., Carbonel P., Kaczmarska I., de Deckker P., Soulié-Marsche I., Callot Y. & Dupeuble P.A. (1987) Biological remains, geochemistry and stable isotopes for the reconstruction of environmental and hydrological changes in the Holocene lakes from North Sahara. *Palaeogeography, Palaeoclimatology, Palaeoecology*, **60**, 1–46.

Geske A., Zorlu J., Richter D.K., Buhl D., Niedermayr A. & Immenhauser A. (2012) Impact of diagenesis and low grade metamorphosis on isotope ($\delta^{26}$Mg, $\delta^{13}$C, $\delta^{18}$O and $^{87}$Sr/$^{86}$Sr) and elemental (Ca, Mg, Mn, Fe and Sr) signatures of Triassic sabkha dolomites. *Chemical Geology*, **332–333**, 45–64.

Gilg H.A. (2005) Eine geochemische Studie an Bentoniten und vulkanischen Gläsern des nordalpinen Molassebeckens (Deutschland, Schweiz). Pp. 16–18 in: *Berichte der Deutschen Ton- und Tonmineralgruppe e.V., Beiträge zur Jahrestagung Celle 10.-12. Oktober 2005* (R. Dohrmann, editor). Deutsche Ton- und Tonmineralgruppe, Köln, Germany.

Gilg H.A., Weber B., Kasbohm J. & Frei R. (2003) Isotope geochemistry and origin of illite-smectite and kaolinite from the Seilitz and Kemmlitz kaolin deposits, Saxony, Germany. *Clay Minerals*, **38**, 95–112.

Goldsmith J.R. & Graf D.L. (1958) Structural and compositional variations in some natural dolomites. *The Journal of Geology*, **66**, 678–693.

https://doi.org/10.1180/claymin.2017.052.2.01 Published online by Cambridge University Press

Govindaraju K. (1989) Compilation of working values and sample description for 272 Geostandards. *Geostandards and Geoanalytical Research*, **13**, 1–113.

Graup G., Horn P., Köhler H. & Müller-Sohnius D. (1981) Source material for moldavites and bentonites. *Naturwissenschaften*, **68**, 616–617.

Grim R.E. & Güven N. (1978) Origin of bentonites. Pp. 78–79 in: *Bentonites: Geology, Mineralogy, Properties and Uses* (R.E. Grim & N. Güven, editors). Development in Sedimentology, **24**. Elsevier, Amsterdam.

Hird K. (1985) *Petrography and geochemistry of some Carboniferous and Precambrian dolomites*. Doctoral thesis, Durham University, UK, pp. 340–343.

Horn P., Müller-Sohnius D., Köhler H. & Graup G. (1985) Rb-Sr systematics of rocks related to the Ries Crater, Germany. *Earth and Planetary Science Letters*, **75**, 384–392.

Horwitz E.P., Chiarizia R. & Dietz M.L. (1992) A novel strontium-selective extraction chromatographic resin. *Solvent Extraction and Ion Exchange*, **10**, 313–336.

Hugget J. & Cuadros J. (2005) Low-temperature illitization of smectite in the Late Eocene and Early Oligocene of the Isle of Wight (Hampshire basin), U.K. *American Mineralogist*, **90**, 1192–1202.

Imai N., Terashima S., Itoh S. & Ando A. (1995) Compilation of analytical data for minor and trace elements in seventeen GSJ geochemical reference samples, "igneous rock series". *Geostandards Newsletter*, **19**, 135–213.

Jin L., Williams E.L., Szramek K.J., Walter L.M. & Hamilton S.K. (2008) Silicate and carbonate mineral weathering in soil profiles developed on Pleistocene glacial drift (Michigan, USA): mass balances based on soil water geochemistry. *Geochimica et Cosmochimica Acta*, **72**, 1027–1042.

Kainzmaier B., Thom, P., Wrobel M. & Pukowietz C. (2007) Geowissenschaftliche Landesaufnahme in der Planungsregion 13 Landshut. Pp. 81–88 in: *Erläuterungen zur Hydrogeologischen Karte 1:100000* (B. Wagner, editor). Bayerischen Geologisches Landesamt, Augsburg, Germany.

Kallis P., Bleich K.E. & Stahr K. (2000) Micromorphological and geochemical characterisation of Tertiary 'freshwater carbonates' locally preserved north of the edge of the Miocene Molasse Basin (SW Germany). *Catena*, **41**, 19–42.

Knechtel M.M. & Patterson S.H. (1956) Bentonite deposits in marine Cretaceous Formations, Hardin District, Montana and Wyoming. *US Geological Survey Bulletin*, **1023**, 1–116.

Knechtel M.M. & Patterson S.H. (1962) Bentonite deposits of the Northern Black Hills District, Wyoming, Montana and South Dakota. *US Geological Survey Bulletin*, **1082-M**, 893–1030.

Köhler H., Frank, C., Königsberger T. & Schön B. (2008) Isotopische (Sr, Nd) Charakterisierung und Datierung Variskischer Granitoide der Moldanubischen Kruste Nordostbayerns. *Geologica Bavarica*, **110**, 170–203.

Köster M.H. & Gilg H.A. (2015) Pedogenic, palustrine and groundwater dolomite formation in non-marine bentonites (Bavaria, Germany). *Clay Minerals*, **50**, 163–183.

Kralik M. (1983) Interpretation of K-Ar and Rb-Sr data from fine fractions of weakly metamorphosed shales and carbonate rocks at the base of the Northern Calcareous Alps (Salzburg, Austria). *Tschermaks Mineralogische und Petrographische Mitteilungen*, **32**, 49–67.

Kretz R. (1982) A model for the distribution of trace elements between calcite and dolomite. *Geochimica et Cosmochimica Acta*, **46**, 1979–1981.

Last W.M. (1980) *Sedimentology and postglacial history of Lake Manitoba*. PhD thesis, University of Manitoba, Winnipeg, Canada, 687 pp.

Last W.M. (1990) Lacustrine dolomite – an overview of modern, Holocene, and Pleistocene occurrences. *Earth-Science Reviews*, **27**, 221–263.

Laudelout H., van Bladel R., Bolt G.H. & Page A.L. (1968) Thermodynamics of heterovalent cation exchange reaction in a montmorillonite clay. *Transactions of the Faraday Society*, **64**, 1477–1488.

Lemcke K. (1973) Zur nachpermischen Geschichte des nördlichen Alpenvorlandes. *Geologica Bavarica*, **69**, 5–48.

Lemcke K. (1988) *Geologie von Bayern. Bd.1. Das Bayerische Alpenvorland vor der Eiszeit*. Schweizerbart'sche Verlagsbuchhandlung, Stuttgart, Germany, 175 pp.

Lohmann K.C. (1988) Geochemical patterns of meteoric diagenetic systems and their application to studies of paleokarst. Pp. 58–80 in: *Paleokarst* (N.P. James & P. W. Choquette, editors). Springer-Verlag, New York.

Lorens R.B. (1981) Sr, Cd, Mn and Co distribution coefficients in calcite as a function of calcite precipitation rate. *Geochimica et Cosmochimica Acta*, **45**, 553–561.

Ludwig K.R. (2008) *User's Manual for Isoplot 3.70. A Geochronological Toolkit for Microsoft Excel*. Berkeley Geochronology Center Special Publication, 4, 76 pp.

Lumsden D.N. & Chimahusky J.S. (1980) Relationship between dolomite nonstoichiometry and carbonate facies parameters. Pp. 123–137 in: *Concepts and Models of Dolomitization* (D.H. Zenger, J.B. Dunham & R.L. Ethington, editors). Special Publication No. **28**, Society of Economic Palaeontologists and Mineralogists, Tulsa, Oklahoma, USA.

Maurer H. & Buchner E. (2007) Identification of fluvial architectural elements of meandering systems by paleosols (Upper Freshwater Molasse, North Alpine

https://doi.org/10.1180/claymin.2017.052.2.01 Published online by Cambridge University Press

Foreland Basin, SW-Germany). *Zeitschrift der Deutschen Gesellschaft für Geowissenschaften*, **158**, 271–285.

McArthur J.M., Howarth R.J. & Bailey T.R. (2001) Strontium isotope stratigraphy: LOWESS Version 3: best fit to the marine Sr-isotope curve for 0–509 Ma and accompanying look-up table for deriving numerical age. *The Journal of Geology*, **109**, 155–170.

Möller P., Morteani G. & Dulski P. (1984) The origin of the calcites from the Pb–Zn veins in the Harz Mountains, Federal Republic of Germany. *Chemical Geology*, **45**, 91–112.

Moore D.M. & Reynolds R.C. (1997) *X-Ray Diffraction and the Identification and Analysis of Clay Minerals*. Oxford University Press, New York, 378 pp.

Müller G., Irion G. & Förstner U. (1972) Formation and diagenesis of inorganic Ca–Mg carbonates in the lacustrine environment. *Naturwissenschaften*, **59**, 158–164.

Nance W.B. & Taylor S.R. (1976) Rare earth element patterns and crustal evolution, I, Australian post-Archean sedimentary rocks. *Geochimica et Cosmochimica Acta*, **40**, 1539–1551.

Nelson C.S. & Smith A.M. (1996) Stable oxygen and carbon isotopes composition fields for skeletal and diagenetic components in New Zealand Cenozoic nontropical carbonate sediments and limestones: a synthesis and review. *New Zealand Journal of Geology and Geophysics*, **39**, 93–107.

Pin C. & Basin C. (1992) Evaluation of a strontium-specific extraction chromatographic method for isotopic analysis in geological materials. *Analytica Chimica Acta*, **269**, 249–255.

Rimstidt J.D., Balog A. & Webb J. (1998) Distribution of trace elements between carbonate minerals and aqueous solutions. *Geochimica et Cosmochimica Acta*, **62**, 1851–1863.

Sánchez-Román M., Romanek C.S., Fernández-Remolar D.C., Sánchez-Navas A., McKenzie J.A., Pibernat R. A. & Vasconcelos C. (2011) Aerobic biomineralization of Mg-rich carbonates: implications for natural environments. *Chemical Geology*, **281**, 143–150.

Sayles F.L. & Mangelsdorf P.C. Jr. (1979) Cation exchange characteristics of Amazon River suspended sediment and its reaction with seawater. *Geochimica et Cosmochimica Acta*, **43**, 767–779.

Schmid W. (2002) Ablagerungsmilieu, Verwitterung und Paläoböden feinklastischer Sedimente der Oberen Süßwassermolasse Bayerns. Bayerische Akademie der Wissenschaften, Heft 172, Doctoral thesis, Ludwig-Maximilians-Universität, Germany, 247 pp.

Schroll E. & Wieden P. (1960) Eine rezente Bildung von Dolomit im Schlamm des Neusiedler Sees. *Tschermaks Mineralogische und Petrographische Mitteilungen*, **7**, 286–289.

Siebel W., Reitter E., Wenzel T. & Blaha U. (2005) Sr isotope systematics of K-feldspars in plutonic rocks revealed by the Rb–Sr microdrilling technique. *Chemical Geology*, **222**, 183–199.

Środoń J. (1980) Precise identification of illite/smectite interstratifications by X-ray powder diffraction. *Clays and Clay Minerals*, **28**, 401–411.

Stanjek H. & Marchel C. (2008) Linking the redox cycles of Fe oxides and Fe-rich clay minerals: an example from a palaeosol of the Upper Freshwater Molasse. *Clay Minerals*, **43**, 69–82.

Tompa É., Nyirő-Kósa I., Rostási Á., Cserny T. & Pósfai M. (2014) Distribution and composition of Mg-calcite and dolomite in the water and sediments of Lake Balaton. *Central European Geology*, **57**, 113–136.

Tucker M.E. & Wright V.P. (1990) *Carbonate Sedimentology*. Blackwell Science, Oxford, UK, pp. 168–172.

Tütken T. & Vennemann T.W. (2009) Stable isotope ecology of Miocene large mammals from Sandelzhausen, southern Germany. *Paläontologische Zeitschrift*, **83**, 207–226.

Tütken T., Vennemann T.W., Janz H. & Heinzmann E.P.J. (2006) Palaeoenvironment and palaeoclimate of the Middle Miocene lake in the Steinheim basin, SW Germany: a reconstruction from C, O, and Sr isotopes of fossil remains. *Palaeogeography, Palaeoclimatology, Palaeoecology*, **241**, 457–491.

Ulbig A. (1994) *Vergleichende Untersuchungen an Bentoniten, Tuffen und sandig-tonigen Einschaltungen in den Bentonitlagerstätten der Oberen Süßwassermolasse*. Doctoral thesis, Technische Universität München, Germany, 245 pp.

Ulbig A. (1999) Untersuchungen zur Entstehung der Bentonite in der bayerischen Oberen Süßwassermolasse. *Neues Jahrbuch Geologisch-Paläontologische Abhandlungen*, **214**, 497–508.

Unger H.J. (1981) Bemerkungen zur stratigraphischen Stellung, der Lagerung und Genese der Bentonitlagerstätten in Niederbayern. *Verhandlungen der Geologischen Bundesanstalt, Wien*, **1981/2**, 193–203.

Unger H.J. (1991) *Geologische Karte von Bayern 1:50000 – Erläuterungen zum Blatt Nr. L 7538 Landshut*. Bayerisches Geologisches Landesamt, München, Germany, 213 pp.

Unger H.J. (1996) Östliche Vorlandmolasse und Braunkohlentertiär i. w. S. Pp. 168–185 in: *Geologische Karte von Bayern 1:500000* (W. Freudenbacher & K. Schwerd, editors). Bayerisches Geologisches Landesamt, München, Germany.

Unger H.J. (1999) Die tektonischen Strukturen der bayerischen Ostmolasse. *Documenta Naturae*, **125**, 1–16.

Unger H.J. & Niemeyer A. (1985) Bentonitlagerstätten zwischen Mainburg und

https://doi.org/10.1180/claymin.2017.052.2.01 Published online by Cambridge University Press

Landshut und ihre zeitliche Einstufung. *Geologisches Jahrbuch*, **D71**, 59–93.

Unger H.J., Fiest W. & Niemeyer A. (1990) Die Bentonite der ostbayerischen Molasse und ihre Beziehungen zu den Vulkaniten des Pannonischen Beckens. *Geologisches Jahrbuch*, **D96**, 55–66.

Vahrenkamp V.C. & Swart P.K. (1990) New distribution coefficient for the incorporation of strontium into dolomite and its implications for the formation of ancient dolomites. *Geology*, **18**, 387–391.

van Lith Y., Warthmann R., Vasconcelos C. & McKenzie J.A. (2003) Sulphate-reducing bacteria induce low-temperature Ca-dolomite and high Mg-calcite formation. *Geobiology*, **1**, 71–79.

Voerkelius S., Lorenz G.D., Rummel S., Quétel C.R., Heiss G., Baxter M., Brach-Papa C., Deters-Itzelsberger P., Hoelzl S., Hoogewerff J., Ponzevera E., Bocxstaele M.V. & Ueckermann H. (2010) Strontium isotopic signatures of natural mineral waters, the reference to a simple geological map and its potential for authentication of food. *Food Chemistry*, **118**, 933–940.

Vogt K. (1980) Bentonite deposits in Lower Bavaria. *Geologisches Jahrbuch*, **D39**, 47–68.

Vogt K. & Köster H.M. (1978) Zur Mineralogie, Kristallchemie und Geochemie einiger Montmorillonite aus Bentoniten. *Clay Minerals*, **13**, 25–43.

Waber H.N., Heidinger M., Lorenz G. & Traber D. (2014) Hydrochemie und Isotopenhydrogeologie von Tiefengrundwässern in der Nordschweiz und im angrenzenden Süddeutschland. *Nagra Arbeitsbericht*, **NAB 13–63**, 1–247.

Wagner B., Töpfner C., Lischeid G., Scholz M., Klinger R. & Klaas P. (2003) Hydrogeochemische Hintergrundwerte der Grundwässer Bayerns. *GLA-Fachberichte*, **21**, 1–250.

Zorlu J. (2007) *Sedimentpetrographische und geochemische Untersuchungen an unterschiedlich überprägten Triasdolomiten der Ost- und Südalpen*. Doctoral thesis, Ruhr-Universität Bochum, Germany, 180 pp.

https://doi.org/10.1180/claymin.2017.052.2.01 Published online by Cambridge University Press